

On Distributed Vector Estimation for Power and Bandwidth Constrained Wireless Sensor Networks

Alireza Sani, *Student Member, IEEE*, Azadeh Vosoughi, *Senior Member, IEEE*,

Abstract—We consider distributed estimation of a Gaussian vector with a linear observation model in an inhomogeneous wireless sensor network, where a fusion center (FC) reconstructs the unknown vector, using a linear estimator. Sensors employ uniform multi-bit quantizers and binary PSK modulation, and communicate with the FC over orthogonal power- and bandwidth-constrained wireless channels. We study transmit power and quantization rate (measured in bits per sensor) allocation schemes that minimize mean-square error (MSE). In particular, we derive two closed-form upper bounds on the MSE, in terms of the optimization parameters and propose “coupled” and “decoupled” resource allocation schemes that minimize these bounds. We show that the bounds are good approximations of the simulated MSE and the performance of the proposed schemes approaches the clairvoyant centralized estimation when total transmit power or bandwidth is very large. We study how the power and rate allocation are dependent on sensors’ observation qualities and channel gains, as well as total transmit power and bandwidth constraints. Our simulations corroborate our analytical results and illustrate the superior performance of the proposed algorithms.

Index Terms—Distributed estimation, Gaussian vector, upper bounds on MSE, power and rate allocation, ellipsoid method, quantization, linear estimator, linear observation model.

I. INTRODUCTION

Distributed parameter estimation problem for wireless sensor networks (WSNs) has a rich literature in signal processing community. Several researchers study quantization design, assuming that sensors’ observations are sent over bandwidth constrained (otherwise error-free) communication channels, examples are [3]–[9]. In particular, [3] designs the optimal quantizers which maximize Bayesian Fisher information, for estimating a random parameter. Assuming identical one-bit quantizers, [8], [9] find the minimum achievable Cramér-Rao lower bound (CRLB) and the optimal quantizers, for estimating a deterministic parameter. The authors in [4], [5] investigate one-bit quantizers for estimating a deterministic parameter, when the FC employs maximum-likelihood estimator. For estimating a random parameter with uniform variable rate quantizers, [6] studies the tradeoff between quantizing a few sensors finely or as many sensors as possible coarsely and its effect on Fisher information, subject to a total rate constraint. For estimating a deterministic parameter [7] investigates a bit allocation scheme that minimizes the mean square error (MSE) when the FC utilizes best linear unbiased estimator (BLUE), subject to a total bit constraint. Several researchers relax the assumption on communication channels being error-free [10],

[11]. For estimating a vector of deterministic parameters, [10] studies an expectation-maximization algorithm and the CRLB, when sensors employ fixed and identical multi-bit quantizers and communication channel model is additive white Gaussian noise (AWGN). A related problem is studied in [11], in which the FC employs a spatial BLUE for field reconstruction and the MSE is compared with a posterior CRLB.

Recent years have also witnessed a growing interest in studying energy efficient distributed parameter estimation for WSNs, examples are [12]–[14]. For estimating a deterministic parameter [12] explores the optimal power allocation scheme which minimizes total transmit power of the network, subject to an MSE constraint, when the FC utilizes BLUE and sensors digitally transmit to the FC over orthogonal AWGN channels. A converse problem is considered in [13], where the authors minimize the MSE, subject to a total transmit power constraint. For a homogeneous WSN, [14] investigates a bit and power allocation scheme that minimizes the MSE, subject to a total transmit power constraint, when communication channels are modeled as binary symmetric channels. We note that [12]–[14] do not include a total bit constraint in their problem formulations. There is a collection of elegant results on energy efficient distributed parameter estimation with analog transmission, also known as Amplify-and-Forward (AF), examples are [15]–[19]. However, the problem formulations in these works naturally cannot have a bandwidth constraint.

Different from the aforementioned works, that consider either transmit power or bandwidth constraint, we consider distributed parameter estimation, subject to both total transmit power and bandwidth constraints. Similar to [4], [5], [7], we choose total number of bits allowed to be transmitted by all sensors to the FC as the measure of total bandwidth. From practical perspectives, having a total transmit power constraint enhances energy efficiency in battery-powered WSNs. Putting a cap on total bandwidth can further improve energy efficiency, since data communication is a major contributor to the network energy consumption. Our new constrained problem formulation allows us to probe the impacts of both constraints on resource allocation and overall estimation accuracy, and enables us to find the best resource allocation (i.e., power and bit) in extreme cases where: (i) we have scarce total transmit power and ample total bandwidth, (ii) we have plentiful total transmit power and scarce total bandwidth. The paper organization follows. Section II introduces our system model and set up our optimization problem. In Section III we derive two closed-form upper bounds, \mathcal{D}_a and \mathcal{D}_b , on the MSE corresponding to the linear estimator at the FC, in terms of the optimization parameters (i.e., transmit power

Part of this research is presented at 48th Asilomar Conference on Signals, Systems and Computers, 2014, and 34th Military Communication, 2015 [1], [2]. This research is supported by NSF under grants CCF-1336123, CCF-1341966, and CCF-1319770.

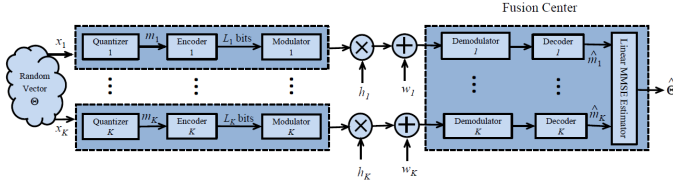


Fig. 1: Our system model consists of K sensors and a FC, tasked with estimating a Gaussian vector θ .

and quantization rate per sensor). In Section IV we propose “coupled” resource allocation schemes that minimize these bounds, utilizing the iterative ellipsoid method. This method conducts multi-dimensional search to find the quantization rate vector. In Section V we propose “decoupled” resource allocation schemes, which rely on one-dimensional search to find the quantization rates. Section VI discusses our numerical results. Section VII concludes our work.

II. SYSTEM MODEL AND PROBLEM STATEMENT

We consider a wireless network with K spatially distributed inhomogeneous sensors. Each sensor makes a noisy observation, which depends on an unobservable vector of random parameters θ , processes locally its observation, and transmits a summary of its observation to a fusion center (FC) over erroneous wireless channels. The FC is tasked with estimating θ , via fusing the collective received data from sensors (see Fig.1). We assume $\theta = [\theta_1, \dots, \theta_q]^T \in \mathbb{R}^q$ is zero-mean Gaussian with covariance matrix $\mathcal{C}_\theta = \mathbb{E}\{\theta\theta^T\}$. Let random scalar x_k denote the noisy observation of sensor k . We assume the following linear observation model:

$$x_k = \mathbf{a}_k^T \theta + n_k, \quad k = 1, \dots, K, \quad (1)$$

where $\mathbf{a}_k = [a_{k1}, \dots, a_{kq}]^T \in \mathbb{R}^q$ is known observation gain vector and $n_k \sim \mathcal{N}(0, \sigma_{n_k}^2)$ is observation noise. We assume n_k 's are mutually uncorrelated and also are uncorrelated with θ . Define observation vector $\mathbf{x} = [x_1, \dots, x_K]^T$, matrix $\mathbf{A} = [\mathbf{a}_1, \dots, \mathbf{a}_K]$, and diagonal covariance matrix $\mathcal{C}_n = \text{diag}(\sigma_{n_1}^2, \dots, \sigma_{n_K}^2)$. Suppose $\mathcal{C}_x = \mathbb{E}\{\mathbf{x}\mathbf{x}^T\}$ and $\mathcal{C}_{x\theta} = \mathbb{E}\{\mathbf{x}\theta^T\}$, respectively, represent the covariance matrix of \mathbf{x} and cross-covariance matrix of \mathbf{x} and θ . It is easy to verify:

$$\mathcal{C}_{x\theta} = \mathbf{A}^T \mathcal{C}_\theta, \quad \mathcal{C}_x = \mathbf{A}^T \mathcal{C}_\theta \mathbf{A} + \mathcal{C}_n.$$

Sensor k employs a uniform quantizer with M_k quantization levels and quantization step size Δ_k , to map x_k into a quantization level $m_k \in \{m_{k,1}, \dots, m_{k,M_k}\}$, where $m_{k,i} = \frac{(2i-1-M_k)\Delta_k}{2}$ for $i = 1, \dots, M_k$. Considering our observation model, we assume x_k lies in the interval $[-\tau_k, \tau_k]$ almost surely, for some reasonably large value of τ_k , i.e., the probability $p(|x_k| \geq \tau_k) \approx 0$. Consequently, we let $\Delta_k = \frac{2\tau_k}{M_k-1}$. These imply that, the quantizer maps x_k as the following: if $x_k \in [m_{k,i} - \frac{\Delta_k}{2}, m_{k,i} + \frac{\Delta_k}{2}]$, then $m_k = m_{k,i}$, if $x_k \geq \tau_k$, then $m_k = \tau_k$, and if $x_k \leq -\tau_k$, then $m_k = -\tau_k$. Following quantization, sensor k maps the index i of $m_{k,i}$ into a bit sequence of length $L_k = \log_2 M_k$, and finally modulates these L_k bits into L_k binary PSK (BPSK) modulated symbols [14]. Sensors send their symbols to the FC over orthogonal wireless channels, where transmission is subject to both transmit power

and bandwidth constraints. The L_k symbols sent by sensor k experience flat fading with a fading coefficient h_k and are corrupted by a zero mean complex Gaussian receiver noise w_k with variance $\sigma_{w_k}^2$. We assume w_k 's are mutually uncorrelated and h_k does not change during the transmission of L_k symbols. Let P_k denote the transmit power corresponding to L_k symbols from sensor k , which we assume it is distributed equally among L_k symbols. Suppose there are constraints on the total transmit power and bandwidth of this network, i.e., $\sum_{k=1}^K P_k \leq P_{tot}$ and $\sum_{k=1}^K L_k \leq B_{tot}$.

In the absence of knowledge of the joint distribution of \mathbf{x} and θ , we resort to linear estimators [13], [17], that only require knowledge of \mathbf{A} and second-order statistics \mathcal{C}_θ and \mathcal{C}_n , to estimate θ with low computational complexity. To describe the operation of linear estimator at the FC, let \hat{m}_k denote the recovered quantization level corresponding to sensor k , where in general $\hat{m}_k \neq m_k$, due to communication channel errors. The FC first processes the received signals from the sensors individually, to recover the transmitted quantization levels. Having $\hat{m}_1, \dots, \hat{m}_K$, the FC applies a linear estimator to form the estimate $\hat{\theta}$. Let $\mathcal{D}_0 = \mathbb{E}\{(\hat{\theta} - \theta)(\hat{\theta} - \theta)^T\}$ denote the error correlation matrix corresponding to this linear estimator, whose i -th diagonal entry, $[\mathcal{D}_0]_{i,i}$, is the MSE corresponding to the i -th entry of vector θ . We choose $\mathcal{D}_0 = \text{tr}(\mathcal{D}_0)$ as our MSE distortion metric [20]. Our goal is to find the optimal resource allocation scheme, i.e., quantization rate L_k and transmit power $P_k \forall k$, that minimize \mathcal{D}_0 . In other words, we are interested to solve the following optimization problem:

$$\begin{aligned} & \underset{L_k, P_k, \forall k}{\text{minimize}} \quad \mathcal{D}_0(\{L_k, P_k\}_{k=1}^K) \\ & \text{s.t.} \quad \sum_{k=1}^K L_k \leq B_{tot}, \quad \sum_{k=1}^K P_k \leq P_{tot}, \quad L_k \in \mathbb{Z}_+, \quad P_k \in \mathbb{R}_+, \quad \forall k. \end{aligned} \quad (2)$$

III. CHARACTERIZATION OF MSE

We wish to characterize \mathcal{D}_0 in terms of the optimization parameters $\{L_k, P_k\}_{k=1}^K$. To accomplish this, we take a two-step approach [12]: in the first step, we assume that the quantization levels transmitted by the sensors are received error-free at the FC. Based on the error-free transmission assumption, we characterize the MSE, due to observation noises and quantization errors. In the second step, we take into account the contribution of wireless communication channel errors on the MSE. This approach provide us with an upper bound on \mathcal{D}_0 , which can be expressed in terms of $\{L_k, P_k\}_{k=1}^K$. Define vector $\mathbf{m} = [m_1, \dots, m_K]^T$, including transmitted quantization levels for all sensors, and vector $\hat{\mathbf{m}} = [\hat{m}_1, \dots, \hat{m}_K]^T$, consisting of recovered quantization levels at the FC. Let:

$$\check{\theta} = \mathbf{G}\mathbf{m}, \quad \text{where } \mathbf{G} = \mathbb{E}\{\theta\mathbf{m}^T\}(\mathbb{E}\{\mathbf{m}\mathbf{m}^T\})^{-1}. \quad (3)$$

Note that $\check{\theta}$ is the linear minimum MSE (LMMSE) estimator, had the FC received the transmitted quantization levels error-free [20]. Having $\hat{\mathbf{m}}$, the FC employs the same linear operator \mathbf{G} to obtain the linear estimate $\hat{\theta} = \mathbf{G}\hat{\mathbf{m}}$. To characterize the MSE, we define covariance matrices $\mathcal{D}_1 = \mathbb{E}\{(\check{\theta} - \theta)(\check{\theta} - \theta)^T\}$ and $\mathcal{D}_2 = \mathbb{E}\{(\hat{\theta} - \check{\theta})(\hat{\theta} - \check{\theta})^T\}$. One can verify:

$$\mathcal{D}_0 = \mathcal{D}_1 + \mathcal{D}_2 + 2\mathbb{E}\{(\check{\theta} - \theta)(\hat{\theta} - \check{\theta})^T\},$$

or equivalently:

$$\mathcal{D}_0 = \mathcal{D}_1 + \mathcal{D}_2 + 2\mathbb{E}\{(\tilde{\boldsymbol{\theta}} - \boldsymbol{\theta})^T(\hat{\boldsymbol{\theta}} - \tilde{\boldsymbol{\theta}})\},$$

where $\mathcal{D}_1 = \text{tr}(\mathcal{D}_1)$ and $\mathcal{D}_2 = \text{tr}(\mathcal{D}_2)$. Applying Cauchy-Schwarz inequality and using the fact $(x+y)^2 \leq 2(x^2+y^2)$ for $x, y \geq 0$, we establish an upper bound on \mathcal{D}_0 as the following:

$$\mathcal{D}_0 \leq (\sqrt{\mathcal{D}_1} + \sqrt{\mathcal{D}_2})^2 \leq 2(\mathcal{D}_1 + \mathcal{D}_2) = 2\mathcal{D}. \quad (4)$$

Note that the upper bound on \mathcal{D}_0 in (4) consists of two terms: the first term $2\mathcal{D}_1$ represents the MSE due to observation noises and quantization errors, whereas the second term $2\mathcal{D}_2$ is the MSE due to communication channel errors. In other words, *the contributions of observation noises and quantization errors in the upper bound are decoupled from those of communication channel errors.*

Relying on (4), in the remaining of this section we derive two upper bounds on \mathcal{D} , denoted as \mathcal{D}_a and \mathcal{D}_b , respectively, in sections III-A and III-B, in terms of $\{L_k, P_k\}_{k=1}^K$. While \mathcal{D}_a is a tighter bound than \mathcal{D}_b , its minimization demands a higher computational complexity. Leveraging on \mathcal{D}_a and \mathcal{D}_b expressions derived in this section, in sections IV and V, we propose two distinct schemes, which we refer to as ‘‘coupled’’ and ‘‘decoupled’’ schemes, to tackle the optimization problem formulated in (2), when \mathcal{D}_0 is replaced with \mathcal{D}_a or \mathcal{D}_b .

A. Characterization of First Bound \mathcal{D}_a

Recall $\mathcal{D} = \mathcal{D}_1 + \mathcal{D}_2$ in (4). Below, we first derive \mathcal{D}_1 . Deriving an exact expression for \mathcal{D}_2 remains elusive. Hence we derive an upper bound on \mathcal{D}_2 , represented as \mathcal{D}_2^{upb} . Let $\mathcal{D}_a = \mathcal{D}_1 + \mathcal{D}_2^{upb}$. Based on (4), we have $\mathcal{D}_0 \leq 2\mathcal{D} \leq 2\mathcal{D}_a$.

• **Derivation of \mathcal{D}_1 in \mathcal{D}_a :** Since $\hat{\boldsymbol{\theta}}$ is the linear MMSE estimator of $\boldsymbol{\theta}$ given \mathbf{m} , \mathcal{D}_1 is the corresponding error covariance matrix. Consequently $\mathcal{D}_1 = \text{tr}(\mathcal{D}_1)$ is [20]:

$$\mathcal{D}_1 = \text{tr}(\mathcal{C}_\theta - \mathbb{E}\{\boldsymbol{\theta}\mathbf{m}^T\}(\mathbb{E}\{\mathbf{m}\mathbf{m}^T\})^{-1}\mathbb{E}\{\boldsymbol{\theta}\mathbf{m}^T\}^T), \quad (5)$$

where $\mathbb{E}\{\boldsymbol{\theta}\mathbf{m}^T\}$ and $\mathbb{E}\{\mathbf{m}\mathbf{m}^T\}$, respectively, are cross-covariance and covariance matrices. To find these matrices, we need to delve into statistics of quantization errors. For sensor k , let the difference between observation x_k and its quantization level m_k , i.e., $\epsilon_k = x_k - m_k$ be the corresponding quantization noise. In general, ϵ_k 's are mutually correlated and also are correlated with x_k 's. However, in [21] it is shown that, when correlated Gaussian random variables are quantized with uniform quantizers of step sizes Δ_k 's, quantization noises can be approximated as mutually independent random variables, that are uniformly distributed in the interval $[-\frac{\Delta_k}{2}, \frac{\Delta_k}{2}]$, and are also independent of quantizer inputs. In this work, since $\boldsymbol{\theta}$ and n_k 's in (1) are assumed Gaussian, x_k 's are correlated Gaussian that are quantized with uniform quantizers of quantization step sizes Δ_k 's. Hence, ϵ_k 's are approximated as mutually independent zero mean uniform random variables with variance $\sigma_{\epsilon_k}^2 = \frac{\Delta_k^2}{12}$, that are also independent of x_k 's (and thus independent of $\boldsymbol{\theta}$ and n_k 's). These imply $\mathbb{E}\{\boldsymbol{\theta}m_k\} = \mathbb{E}\{\boldsymbol{\theta}(x_k - \epsilon_k)\} = \mathcal{C}_\theta \mathbf{a}_k$. Therefore:

$$\mathbb{E}\{\boldsymbol{\theta}\mathbf{m}^T\} = \mathcal{C}_\theta \mathbf{A} = \mathcal{C}_{x\theta}^T. \quad (6)$$

Also, it is straightforward to verify:

$$\mathbb{E}\{\mathbf{m}\mathbf{m}^T\} = \mathbf{A}^T \mathcal{C}_\theta \mathbf{A} + \mathcal{C}_n + \mathbf{Q} = \mathcal{C}_x + \mathbf{Q}, \quad (7)$$

where $\mathbf{Q} = \text{diag}(\sigma_{\epsilon_1}^2, \dots, \sigma_{\epsilon_K}^2)$. Substituting (6), (7) into (3), (5) yield:

$$\mathbf{G} = \mathcal{C}_{x\theta}^T (\mathcal{C}_x + \mathbf{Q})^{-1}, \quad (8)$$

$$\mathcal{D}_1 = \text{tr}(\mathcal{C}_\theta) - \text{tr}(\mathcal{C}_{x\theta}^T (\mathcal{C}_x + \mathbf{Q})^{-1} \mathcal{C}_{x\theta}). \quad (9)$$

• **Derivation of \mathcal{D}_2^{upb} in \mathcal{D}_a :** Substituting $\tilde{\boldsymbol{\theta}} = \mathbf{G}\mathbf{m}$ and $\hat{\boldsymbol{\theta}} = \mathbf{G}\hat{\mathbf{m}}$ in \mathcal{D}_2 we reach $\mathcal{D}_2 = \mathbf{G}\mathcal{M}\mathbf{G}^T$, where we define matrix $\mathcal{M} = \mathbb{E}\{(\hat{\mathbf{m}} - \mathbf{m})(\hat{\mathbf{m}} - \mathbf{m})^T\}$. Since communication channel noises are mutually uncorrelated $\mathbb{E}\{(\hat{m}_i - m_i)(\hat{m}_j - m_j)\} = 0$ for $i \neq j$. Hence \mathcal{M} is a diagonal matrix, whose k -th entry, $[\mathcal{M}]_{k,k} = \mathbb{E}\{(\hat{m}_k - m_k)^2\}$, depends on the employed modulation scheme, channel gain $|h_k|$, channel noise variance $\sigma_{\omega_k}^2$, value of τ_k , transmit power P_k , and quantization rate L_k . For our system model depicted in Section II, in which sensors utilize BPSK modulation, we obtain (see Appendix VIII-A):

$$[\mathcal{M}]_{k,k} \leq \left(\frac{4\tau_k^2 L_k}{3}\right) \exp\left(-\frac{\gamma_k P_k}{L_k}\right) = u_k, \quad (10)$$

where $\gamma_k = \frac{|h_k|^2}{2\sigma_{\omega_k}^2}$ is *channel to noise ratio (CNR)* for sensor k . Since \mathcal{M} and \mathcal{D}_2 are semi-positive definite matrices, i.e., $\mathcal{M} \succeq 0, \mathcal{D}_2 \succeq 0$, the bound in (10) can provide us an upper bound on $\mathcal{D}_2 = \text{tr}(\mathcal{D}_2)$. Let $\mathcal{M}' = \text{diag}(u_1, \dots, u_K)$. Since $\mathcal{M}' - \mathcal{M} \succeq 0$ and $\mathbf{G}\mathcal{M}'\mathbf{G}^T \succeq 0$, we find [22]:

$$\mathcal{D}_2 = \text{tr}(\mathbf{G}\mathcal{M}\mathbf{G}^T) \leq \text{tr}(\mathbf{G}\mathcal{M}'\mathbf{G}^T) = \mathcal{D}_2^{upb}, \quad (11)$$

Regarding \mathcal{D}_1 and \mathcal{D}_2^{upb} a remark follows.

• **Remark 1:** Note \mathcal{D}_1 in (9) only depends on quantization rates L_k 's, through the variances of quantization noises ϵ_k 's in \mathbf{Q} . On the other hand, \mathcal{D}_2^{upb} in (11) depends on transmit powers P_k 's, through \mathcal{M}' , as well as L_k 's through \mathcal{M}' and \mathbf{Q} in \mathbf{G} . Hence, we derive the upper bound $\mathcal{D}_a = \mathcal{D}_1 + \mathcal{D}_2^{upb}$, in terms of the optimization parameters $\{L_k, P_k\}_{k=1}^K$.

B. Characterization of Second Bound \mathcal{D}_b

Recall from Section III-A that $\mathcal{D}_a = \mathcal{D}_1 + \mathcal{D}_2^{upb}$ where $\mathcal{D}_0 \leq 2\mathcal{D} \leq 2\mathcal{D}_a$. Note that both \mathcal{D}_1 and \mathcal{D}_2^{upb} involve inversion of matrix $\mathcal{C}_x + \mathbf{Q}$, incurring a high computational complexity that grows with K . For large K such a matrix inversion, required to find the optimal resource allocation (see Section IV-A), is burdensome. To curtail computational complexity, in this section we derive upper bounds on \mathcal{D}_1 and \mathcal{D}_2^{upb} , represented as \mathcal{D}_1^{upb} and \mathcal{D}_2^{uupb} , respectively, that do not involve such a matrix inversion. Let $\mathcal{D}_b = \mathcal{D}_1^{upb} + \mathcal{D}_2^{uupb}$. Based on (4), we have $\mathcal{D}_0 \leq 2\mathcal{D} \leq 2\mathcal{D}_b$.

• **Derivation of \mathcal{D}_1^{upb} in \mathcal{D}_b :** To find an upper bound on \mathcal{D}_1 in (9) we use the following inequality [16]:

$$\text{tr}(\mathbf{E}^T \mathbf{F}^{-1} \mathbf{E}) \geq \frac{(\text{tr}(\mathbf{E}^T \mathbf{E}))^2}{\text{tr}(\mathbf{E}^T \mathbf{F} \mathbf{E})}, \quad (12)$$

where \mathbf{E} is arbitrary and $\mathbf{F} \succeq 0$. Recall \mathbf{Q} is a diagonal matrix with non-negative entries, i.e., $\mathbf{Q} \succeq 0$. Also, $\mathcal{C}_x \succeq 0$ since it is a covariance matrix. These imply $\mathbf{Q} + \mathcal{C}_x \succeq 0$ [22]. Applying (12) to (9) we reach:

$$\mathcal{D}_1 \leq \text{tr}(\mathcal{C}_\theta) - \frac{(\text{tr}(\mathcal{C}_{x\theta}^T (\mathcal{C}_x + \mathbf{Q}) \mathcal{C}_{x\theta}))^2}{\text{tr}(\mathcal{C}_{x\theta}^T (\mathcal{C}_x + \mathbf{Q}) \mathcal{C}_{x\theta})} = \mathcal{D}_1^{upb}. \quad (13)$$

• **Derivation of \mathcal{D}_2^{upb} in \mathcal{D}_b :** To find an upper bound on \mathcal{D}_2^{upb} in (11), we take the following steps:

$$\begin{aligned} \mathcal{D}_2^{upb} &\stackrel{(a)}{=} \sum_{k=1}^K \lambda_k (\mathbf{G}^T \mathbf{G} \mathcal{M}') \stackrel{(b)}{\leq} \sum_{k=1}^K \lambda_k (\mathbf{G}^T \mathbf{G}) \lambda_k (\mathcal{M}') \\ &\stackrel{(c)}{\leq} \lambda_{max}(\mathbf{G}^T \mathbf{G}) \sum_{k=1}^K \lambda_k (\mathcal{M}') = \lambda_{max}(\mathbf{G}^T \mathbf{G}) \sum_{k=1}^K u_k, \end{aligned} \quad (14)$$

where (a) in (14) is obtained using the facts $\text{tr}(\mathbf{E}\mathbf{F}) = \text{tr}(\mathbf{F}\mathbf{E})$ for arbitrary \mathbf{E}, \mathbf{F} with matching sizes and $\text{tr}(\mathbf{E}) = \sum_k \lambda_k(\mathbf{E}) = \sum_k [\mathbf{E}]_{k,k}$ for a square matrix \mathbf{E} with eigenvalues λ_k 's, (b) is found using Theorem 9 in [23], and (c) is true since $\lambda_k(\mathbf{G}^T \mathbf{G}) \leq \lambda_{max}(\mathbf{G}^T \mathbf{G})$ for $\forall k$. Next, we derive an upper bound on $\lambda_{max}(\mathbf{G}^T \mathbf{G})$ in (14). Using \mathbf{G} in (8) we find $\mathbf{G}^T \mathbf{G} = (\mathbf{C}_x + \mathbf{Q})^{-1} \mathbf{C}_{x\theta} \mathbf{C}_{x\theta}^T (\mathbf{C}_x + \mathbf{Q})^{-1}$. Note $(\mathbf{C}_x + \mathbf{Q})^{-1}$ and $\mathbf{C}_{x\theta} \mathbf{C}_{x\theta}^T$ are symmetric matrices. Therefore:

$$\begin{aligned} \lambda_{max}(\mathbf{G}^T \mathbf{G}) &\stackrel{(d)}{=} \|\mathbf{G}^T \mathbf{G}\|_2 \leq [\|(\mathbf{C}_x + \mathbf{Q})^{-1}\|_2]^2 \|\mathbf{C}_{x\theta} \mathbf{C}_{x\theta}^T\|_2 \\ &= [\lambda_{max}((\mathbf{C}_x + \mathbf{Q})^{-1})]^2 \lambda_{max}(\mathbf{C}_{x\theta} \mathbf{C}_{x\theta}^T) \\ &\stackrel{(e)}{=} \left[\frac{1}{\lambda_{min}(\mathbf{C}_x + \mathbf{Q})} \right]^2 \lambda_{max}(\mathbf{C}_{x\theta} \mathbf{C}_{x\theta}^T) \quad (15) \\ &\stackrel{(f)}{\leq} \left[\frac{1}{\lambda_{min}(\mathbf{C}_x) + \min_k(\sigma_{\epsilon_k}^2)} \right]^2 \lambda_{max}(\mathbf{C}_{x\theta} \mathbf{C}_{x\theta}^T) = \tilde{\lambda}. \end{aligned}$$

(d) holds due to the norm equality [24], (e) is true since $\lambda_{max}(\mathbf{E}^{-1}) = \frac{1}{\lambda_{min}(\mathbf{E})}$ for an invertible \mathbf{E} , and (f) is obtained since for $\mathbf{E}, \mathbf{F} \geq 0$ Weyl's inequality [24] states $\lambda_{min}(\mathbf{E} + \mathbf{F}) \geq \lambda_{min}(\mathbf{E}) + \lambda_{min}(\mathbf{F})$. Also, $\lambda_{min}(\mathbf{Q}) = \min_k(\sigma_{\epsilon_k}^2)$. Combining (14) and (15) we reach:

$$\mathcal{D}_2^{upb} \leq \tilde{\lambda} \sum_{k=1}^K u_k = \mathcal{D}_2^{upb}.$$

Regarding \mathcal{D}_1^{upb} and \mathcal{D}_2^{upb} a remark follows.

• **Remark 2:** Note \mathcal{D}_1^{upb} in (13) only depends on L_k 's, through the variances of quantization noises ϵ_k 's in \mathbf{Q} . On the other hand, \mathcal{D}_2^{upb} depends on P_k 's, through u_k 's, as well as L_k 's through u_k 's and $\sigma_{\epsilon_k}^2$'s in $\tilde{\lambda}$. Hence, we derive the upper bound $\mathcal{D}_b = \mathcal{D}_1^{upb} + \mathcal{D}_2^{upb}$, in terms of $\{L_k, P_k\}_{k=1}^K$.

IV. "COUPLED" SCHEME FOR RESOURCE ALLOCATION

So far, we have established $\mathcal{D}_0 \leq 2\mathcal{D} \leq 2\mathcal{D}_a \leq 2\mathcal{D}_b$, where \mathcal{D}_a and \mathcal{D}_b are derived in sections III-A and III-B, in terms of $\{L_k, P_k\}_{k=1}^K$. In this section we address the optimization problem formulated in (2), when \mathcal{D}_0 is replaced with \mathcal{D}_a (in Section IV-A) or \mathcal{D}_b (in Section IV-C). Note that (2) is a mixed integer nonlinear programming with exorbitant computational complexity [25]. To simplify the problem, we temporarily relax the integer constraint on L_k 's and allow them to be positive numbers, i.e., we consider:

$$\begin{aligned} &\underset{L_k, P_k, \forall k}{\text{minimize}} \mathcal{D}_0(\{L_k, P_k\}_{k=1}^K) \quad (16) \\ &\text{s.t.} \sum_{k=1}^K L_k \leq B_{tot}, \sum_{k=1}^K P_k \leq P_{tot}, L_k, P_k \in \mathbb{R}_+, \forall k. \end{aligned}$$

We propose "coupled" scheme to solve the relaxed problem in (16), where the objective function is replaced with \mathcal{D}_a or \mathcal{D}_b . In Section IV-B we discuss a novel approach to migrate from relaxed continuous L_k 's to integer L_k 's solutions.

A. Coupled Scheme for Minimizing \mathcal{D}_a

The quintessence of this "coupled" scheme follows. We replace \mathcal{D}_0 with \mathcal{D}_a in (16) and decompose the relaxed problem into two sub-problems (SP1) and (SP2) as the following:

$$\text{(SP1)} \quad \text{given} \{L_k\}_{k=1}^K, \underset{P_k, \forall k}{\text{minimize}} \mathcal{D}_a(\{P_k\}_{k=1}^K) \quad (17)$$

$$\text{s.t.} \sum_{k=1}^K P_k \leq P_{tot}, P_k \in \mathbb{R}_+, \forall k,$$

$$\text{(SP2)} \quad \text{given} \{P_k\}_{k=1}^K, \underset{L_k, \forall k}{\text{minimize}} \mathcal{D}_a(\{L_k\}_{k=1}^K) \quad (18)$$

$$\text{s.t.} \sum_{k=1}^K L_k \leq B_{tot}, L_k \in \mathbb{R}_+, \forall k.$$

We iterate between solving these two sub-problems, until we reach the solution.

• **Solving (SP1) Given in (17):** Considering Remark 1, we note that only \mathcal{D}_2^{upb} in \mathcal{D}_a depends on P_k 's. Hence, we replace the objective function in (17) with \mathcal{D}_2^{upb} . Since \mathcal{D}_2^{upb} is a jointly convex function of P_k 's (see Appendix VIII-B) we use Lagrange multiplier method and solve the corresponding Karush-Kuhn-Tucker (KKT) conditions to find the solution. Substituting u_k of (10) into \mathcal{M}' and noting that \mathbf{G} does not depend on P_k 's, we rewrite (SP1) as below:

$$\text{given} \{L_k\}_{k=1}^K, \underset{P_k, \forall k}{\text{minimize}} \sum_{k=1}^K \alpha_k L_k \exp\left(-\frac{\gamma_k P_k}{L_k}\right) \quad (19)$$

$$\text{s.t.} \sum_{k=1}^K P_k \leq P_{tot}, P_k \in \mathbb{R}_+, \forall k,$$

where $\alpha_k = (4\tau_k^2/3) \|\mathbf{g}_k\|^2$ and $\|\mathbf{g}_k\|^2$ is the squared Euclidean norm of the k -th column of \mathbf{G} . Let $\mathcal{L}(\{L_k, P_k, \mu_k\}_{k=1}^K, \lambda)$ be the Lagrangian for (19), where μ_k and λ are the Lagrange multipliers. The corresponding KKT conditions are:

$$\begin{aligned} \frac{\partial \mathcal{L}}{\partial P_k} &= -\alpha_k \gamma_k \exp\left(-\frac{\gamma_k P_k}{L_k}\right) - \mu_k + \lambda = 0, \forall k, \\ P_k \mu_k &= 0, \quad \mu_k \geq 0, \quad P_k \geq 0, \forall k, \\ \lambda \left(\sum_{k=1}^K P_k - P_{tot} \right) &= 0, \quad \lambda \geq 0, \quad \sum_{k=1}^K P_k \leq P_{tot}. \end{aligned}$$

Since \mathcal{D}_2^{upb} is a decreasing function of P_k 's and P_{tot} (see Appendix VIII-B), solving (19) for P_k 's we find:

$$P_k = \left[\frac{L_k}{\gamma_k} \ln\left(\frac{\gamma_k \alpha_k}{\lambda^*}\right) \right]^+, \quad \forall k, \quad (20)$$

where $[x]^+ = \max(0, x)$, $\sum_{k=1}^K P_k = P_{tot}$ and $\ln \lambda^*$ is:

$$\ln \lambda^* = \left(\sum_{k \notin \mathcal{I}} \frac{L_k}{\gamma_k} \right)^{-1} [-P_{tot} + \sum_{k \notin \mathcal{I}} \frac{L_k}{\gamma_k} \ln(\gamma_k \alpha_k)]. \quad (21)$$

Set $\mathcal{I} = \{k : P_k = 0, k = 0, \dots, K\}$ in (21) is the set of inactive sensors: sensors whose $L_k = 0$ or $\gamma_k \alpha_k < \lambda^*$, where γ_k is CNR of sensor k and α_k depends on the parameters of the observation model. Eq. (20) indicates that P_k depends on both sensor observation and communication channel qualities, through γ_k and α_k . Also, sensor k with a larger L_k is allocated

a larger P_k . For asymptotic regime of large P_{tot} , we substitute (21) into (20) and let $P_{tot} \rightarrow \infty$ to reach the following:

$$P_k = \frac{L_k P_{tot}}{\gamma_k \sum_{k \notin \mathcal{I}} \frac{L_k}{\gamma_k}}, \quad \forall k. \quad (22)$$

Eq. (22) implies in this asymptotic regime, P_k is proportional to $\frac{L_k}{\gamma_k}$. When L_k 's are equal, sensor with a smaller CNR is allotted a larger P_k (inverse of water-filling). When γ_k 's are equal, sensor with a larger L_k is assigned a larger P_k . Regarding the solution in (20) two remarks follow.

• **Remark 3:** For sensor k , we examine how P_k varies as γ_k changes, for a given L_k . We obtain:

$$\frac{\partial P_k}{\partial \gamma_k} = \frac{L_k}{\gamma_k^2} (1 - \ln(\frac{\gamma_k \alpha_k}{\lambda^*})), \quad \forall k. \quad (23)$$

Examining (23) shows when $\gamma_k \alpha_k < e\lambda^*$, as γ_k increases P_k increases (water-filling). On the other hand, when $\gamma_k \alpha_k > e\lambda^*$, as γ_k increases P_k decreases (inverse of water-filling).

• **Remark 4:** For sensors i, j we examine how P_i, P_j are related to γ_i, γ_j . Suppose $L_i = L_j = L$ and $\alpha_i = \alpha_j = \alpha$. When $\frac{e\lambda^*}{\alpha} < \gamma_j < \gamma_i$ then $P_i < P_j$ (inverse of water-filling). On the other hand, when $\gamma_j < \gamma_i < \frac{e\lambda^*}{\alpha}$ then $P_i > P_j$ (water-filling).

• **Solving (SP2) Given in (18):** Finding a closed-form solution for this problem remains elusive, due to non-linearity of the cost function and the fact that the inequality constraint on L_k 's is not necessarily active. Let $\mathcal{F} = \{L_k : \sum_{k=1}^K L_k \leq B_{tot}, L_k \in \mathbb{R}_+, \forall k\}$ be the feasible set of (SP2). To solve (SP2) we use a *modified version of Ellipsoid method* [26]. This cutting-plane optimization method is the generalized form of the one-dimensional bisection method for higher dimensions, and is theoretically efficient with guaranteed convergence [26]. The description of the method follows. Suppose the solution of (SP2) is contained in an initial ellipsoid ϵ^0 with center $\mathbf{L}'^{(0)}$ and shaped by matrix $\mathbf{S}^{(0)} \succeq 0$. The definition of ϵ^0 is:

$$\epsilon^0 = \{\mathbf{z} : (\mathbf{z} - \mathbf{L}'^{(0)})^T \mathbf{S}^{(0)-1} (\mathbf{z} - \mathbf{L}'^{(0)}) \leq 1\}.$$

For ϵ^0 we choose a sphere that contains \mathcal{F} , with center $\mathbf{L}'^{(0)} = \frac{B_{tot}}{2} [1, \dots, 1]$, radius $\frac{B_{tot}}{2} \sqrt{K}$, and thus $\mathbf{S}^{(0)} = (\frac{B_{tot} \sqrt{K}}{2}) \mathbf{I}_K$. Essentially, this method uses gradient evaluation at iteration i , to discard half of ϵ^i and to form ϵ^{i+1} with center $\mathbf{L}'^{(i+1)}$, which is the minimum volume ellipsoid covering the remaining half of ϵ^i . Note that ϵ^{i+1} can be larger than ϵ^i in diameter, however, it is proven that the volume of ϵ^{i+1} is smaller than that of ϵ^i and center $\mathbf{L}'^{(i)}$ eventually converges to the solution of (SP2). To elaborate this method, suppose at iteration i , we have ellipsoid ϵ^i with center $\mathbf{L}'^{(i)}$ and shaped by matrix $\mathbf{S}^{(i)}$. Ellipsoid ϵ^{i+1} at iteration $i+1$ is obtained by evaluating the gradient $\nabla^{(i)}$, defined below. When $\mathbf{L}'^{(i)} \in \mathcal{F}$ then $\nabla^{(i)}$ is the gradient of the objective function (so-called objective cut) evaluated at $\mathbf{L}'^{(i)}$. When $\mathbf{L}'^{(i)} \notin \mathcal{F}$ then $\nabla^{(i)}$ is the gradient of the inequality constraint that is being violated (so-called feasibility cut) evaluated at $\mathbf{L}'^{(i)}$. The update steps

are:

$$\begin{aligned} \epsilon^{i+1} &= \epsilon^i \cap \{\mathbf{z} : \nabla^{(i)T} (\mathbf{z} - \mathbf{L}'^{(i)}) \leq 0\}, \\ \mathbf{L}'^{(i+1)} &= \mathbf{L}'^{(i)} - \frac{1}{K+1} \mathbf{S}^{(i)} \tilde{\nabla}^{(i)}, \quad \tilde{\nabla}^{(i)} = \frac{\nabla^{(i)}}{\sqrt{\nabla^{(i)T} \mathbf{S}^{(i)} \nabla^{(i)}}}, \\ \mathbf{S}^{(i+1)} &= \frac{K^2}{K^2-1} (\mathbf{S}^{(i)} - \frac{2}{K+1} \mathbf{S}^{(i)} \tilde{\nabla}^{(i)} \tilde{\nabla}^{(i)T} \mathbf{S}^{(i)}), \end{aligned}$$

in which:

$$\nabla^{(i)} = \begin{cases} \nabla_{oc}^{(i)}, & \text{if } \sum_{k=1}^K L_k'^{(i)} \leq B_{tot}, L_k'^{(i)} \in \mathbb{R}_+, \forall k, \\ \nabla_{sfc}^{(i)}, & \text{if } \sum_{k=1}^K L_k'^{(i)} > B_{tot}, L_k'^{(i)} \in \mathbb{R}_+, \forall k, \\ \nabla_{nfc}^{(i)}, & \text{if } L_j'^{(i)} \leq 0, \text{ for some } j \in \{1, \dots, K\}, \end{cases}$$

where $\nabla_{oc}^{(i)}$, $\nabla_{sfc}^{(i)}$ and $\nabla_{nfc}^{(i)}$ are objective cut, rate-sum constraint feasibility cut and nonnegative rate feasibility cut, respectively, evaluated at $\mathbf{L}'^{(i)}$:

$$\nabla_{oc}^{(i)} = [\frac{\partial \mathcal{D}_a}{\partial L_1} |_{L_1=L_1'^{(i)}}, \dots, \frac{\partial \mathcal{D}_a}{\partial L_K} |_{L_K=L_K'^{(i)}}]^T, \quad (24)$$

$$\nabla_{sfc}^{(i)} = [\frac{\partial (\sum_{j=1}^K L_j)}{\partial L_1} |_{L_1=L_1'^{(i)}}, \dots, \frac{\partial (\sum_{j=1}^K L_j)}{\partial L_K} |_{L_K=L_K'^{(i)}}]^T \quad (25)$$

$$\nabla_{nfc}^{(i)} = [\frac{-\partial L_j}{\partial L_1} |_{L_1=L_1'^{(i)}}, \dots, \frac{-\partial L_j}{\partial L_K} |_{L_K=L_K'^{(i)}}]^T. \quad (26)$$

After some mathematical manipulations and using the fact $\frac{\partial \mathbf{E}^{-1}}{\partial x} = -\mathbf{E}^{-1} \frac{\partial \mathbf{E}}{\partial x} \mathbf{E}^{-1}$, we find $\frac{\partial \mathcal{D}_a}{\partial L_k} \forall k$ in (24) is equal to below:

$$\text{tr}(\mathbf{G} [\frac{\partial \mathbf{Q}}{\partial L_k} - \frac{\partial \mathbf{Q}}{\partial L_k} (\mathbf{C}_x + \mathbf{Q})^{-1} \mathcal{M}' + \frac{\partial \mathcal{M}'}{\partial L_k} - \mathcal{M}' (\mathbf{C}_x + \mathbf{Q})^{-1} \frac{\partial \mathbf{Q}}{\partial L_k}] \mathbf{G}^T),$$

in which $\frac{\partial \mathbf{Q}}{\partial L_k}$ and $\frac{\partial \mathcal{M}'}{\partial L_k}$ are all-zero matrices, except for one non-zero element in each matrix $[\frac{\partial \mathbf{Q}}{\partial L_k}]_{k,k} = \frac{\partial \sigma_{\epsilon_k}^2}{\partial L_k} = -\frac{2 \ln 2 \tau_k^2 2^{L_k}}{3(2^{L_k}-1)^3}$ and $[\frac{\partial \mathcal{M}'}{\partial L_k}]_{k,k} = \frac{\partial u_k}{\partial L_k} = \frac{4\tau_k^2}{3} \exp(-\frac{\gamma_k P_k}{L_k}) [1 + \frac{\gamma_k P_k}{L_k}]$. Furthermore, $\nabla_{sfc}^{(i)}$ in (25) is a vector of all ones and $\nabla_{nfc}^{(i)}$ in (26) is a vector of all zeros and -1 for its j -th entry. As stopping criterion, we check if $\sqrt{\nabla^{(i)T} \mathbf{S}^{(i)} \nabla^{(i)}} < \epsilon$, where ϵ is a predetermined error threshold, or if the number of iterations exceeds a predetermined maximum I_{max} . Fig. 2 illustrates the above ellipsoid method for $K=2$ sensors, where the feasible set \mathcal{F} is the triangle with the hatch pattern.

In nutshell, we have analytically solved (SP1) and provided an iterative ellipsoid method with guaranteed convergence to address (SP2). With these ammunitions we tackle the problem in (16), when \mathcal{D}_0 is replaced with \mathcal{D}_a . Let vectors $\mathbf{L}^c = [L_1^c, \dots, L_K^c]$, $\mathbf{P}^c = [P_1^c, \dots, P_K^c]$ denote the solutions to (16). We take an iterative approach that switches between solving (SP1) and (SP2), until we converge to vectors \mathbf{L}^c and \mathbf{P}^c . As stopping criterion, we check if the decrease in \mathcal{D}_a in two consecutive iterations is less than a predetermined error threshold η , or if the number of switching between solving (SP1) and (SP2) exceeds a predetermined maximum J_{max} . The “ a -coupled” algorithm summarizes the steps described above, guaranteeing that \mathcal{D}_a decreases in each iteration j . Regarding “ a -coupled” algorithm a remark follows.

• **Remark 5:** Implementing the ellipsoid method requires a K -dimensional search. Also, in inner loop where $\mathbf{L}'^{(i)} \in \mathcal{F}$ we have $\nabla^{(i)} = \nabla_{oc}^{(i)}$, which needs inversion of $\mathbf{C}_x + \mathbf{Q}$. In outer loop inversion of $\mathbf{C}_x + \mathbf{Q}$ is required to update $\alpha_k^{(j)}$.

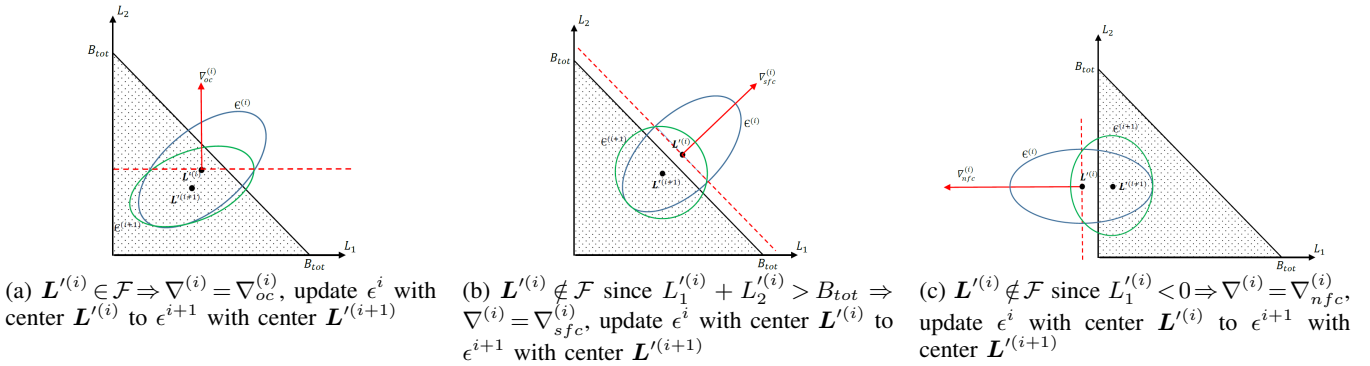


Fig. 2: Modified ellipsoid method for constrained optimization problem

Data: System parameters defined in Section II

Result: Continuous solutions for optimization parameters

$$\mathbf{L}^c = [L_1^c, \dots, L_K^c], \mathbf{P}^c = [P_1^c, \dots, P_K^c]$$

initialization;

$$j = 0, \mathbf{L}^{c(0)} = \frac{B_{tot}}{2} [1, \dots, 1], \mathbf{P}^{c(0)} = [0, \dots, 0]$$

while 1 do

$$\mathbf{G}^{(j)} = \mathbf{C}_{\mathbf{x}\theta}^T (\mathbf{C}_{\mathbf{x}} + \text{diag}(\frac{\tau_1^2}{3(2^{L_1^{(j)}} - 1)^2}, \dots, \frac{\tau_K^2}{3(2^{L_K^{(j)}} - 1)^2}))^{-1}$$

$$\alpha_k^{(j)} = (4\tau_k^2/3) \|\mathbf{g}_k^{(j)}\|^2, \forall k$$

$$P_k^{c(j)} = \left[\frac{L_k^{c(j)}}{\gamma_k} \ln\left(\frac{\gamma_k \alpha_k^{(j)}}{e^{-P_{tot}} \prod_{k \notin \mathcal{I}} (\gamma_k \alpha_k^{(j)}) \frac{L_k^{(j)}}{\gamma_k}} \right) \right]^+$$

 Modified ellipsoid method

modified ellipsoid method initialization;

$$i = 0, \mathbf{L}'^{(0)} = \frac{B_{tot}}{2} [1, \dots, 1], \mathbf{S}^{(0)} = \left(\frac{B_{tot} \sqrt{K}}{2} \right) \mathbf{I}$$

while 1 do

$$\mathbf{L}'^{(i+1)} = \mathbf{L}'^{(i)} - \frac{1}{K+1} \mathbf{S}^{(i)} \tilde{\nabla}^{(i)}$$

$$\mathbf{S}^{(i+1)} = \frac{K^2}{K^2-1} (\mathbf{S}^{(i)} - \frac{2}{K+1} \mathbf{S}^{(i)} \tilde{\nabla}^{(i)} \tilde{\nabla}^{(j)T} \mathbf{S}^{(i)})$$

$$i = i + 1$$

if $\sqrt{\tilde{\nabla}^{(i+1)T} \mathbf{S}^{(i+1)} \tilde{\nabla}^{(i+1)}} < \epsilon \vee i > I_{max}$ **then**
 | break
end

end

$$\mathbf{L}^{c(j+1)} = \mathbf{L}'^{(i+1)}$$

$j = j + 1$

if $\mathcal{D}_a(\mathbf{P}^{c(j)}, \mathbf{L}^{c(j)}) - \mathcal{D}_a(\mathbf{P}^{c(j-1)}, \mathbf{L}^{c(j-1)}) < \eta$

$\vee j > J_{max}$ **then**

| break

end

end

Algorithm: “a-coupled” algorithm for minimizing \mathcal{D}_a

B. Migration from Continuous to Integer Solutions for Rates

We describe an approach on how to migrate from continuous solution \mathbf{L}^c to integer solution \mathbf{L}^d . Let \mathcal{X} be the index set of sensors which quantization rates are discretized. Initially \mathcal{X} is an empty set. We consider two scenarios: (i) $\sum_{j \in \mathcal{X}} L_j^d + \sum_{j \notin \mathcal{X}} L_j^c < B_{tot}$, (ii) $\sum_{j \in \mathcal{X}} L_j^d + \sum_{j \notin \mathcal{X}} L_j^c = B_{tot}$. When case (i) occurs, it means that minimizing \mathcal{D}_a has not been negatively impacted by bandwidth shortage. Hence, we discretize the rate of sensor j with the smallest L_j^c , since this sensor is more likely to be the weakest player in the network, in the sense that it has the minimal contribution to \mathcal{D}_a . We round L_j^c “up” or “down”, depending on which one yields a smaller \mathcal{D}_a and consider the discretized L_j^d as fixed and final value. When case (ii) occurs, it is very likely that minimizing \mathcal{D}_a has been negatively impacted by bandwidth shortage and some sensors

were imposed smaller rates, compared with an unlimited B_{tot} scenario. Note that in case (ii), rounding up the rate of any sensor, would enforce decreasing the rates of some other sensors. Hence, we should discretize in a way that, the positive impact of rounding up a rate on \mathcal{D}_a would dominate the negative effect of decreasing the rates of some other sensors on \mathcal{D}_a . Therefore, we discretize the rate of sensor j with the largest L_j^c , since this sensor is more likely to be the strongest player, in the sense that it has the maximal contribution to \mathcal{D}_a . We round L_j^c “up” and consider the discretized L_j^d as fixed and final value. After each discretization, we need to update \mathcal{X} and the available bandwidth to $B_{tot} - \sum_{j \in \mathcal{X}} L_j^d$, and apply “a-coupled” algorithm to reallocate P_{tot} among all sensors and $B_{tot} - \sum_{j \in \mathcal{X}} L_j^d$ among those sensors with continuous valued rates. We continue this procedure until \mathcal{X} includes all sensors.

C. Coupled Scheme for Minimizing \mathcal{D}_b

Similar to Section IV-A, in this section we consider two sub-problems, which we refer to as (SP3) and (SP4). They are similar to (17) and (18), with the difference that \mathcal{D}_a is replaced with \mathcal{D}_b . Solutions to (SP3) and (SP4) follow.

• **Solving (SP3):** Considering Remark 2, we note that only \mathcal{D}_2^{upb} in \mathcal{D}_b depends on P_k 's. Hence, we replace the objective function in (SP3) with \mathcal{D}_2^{upb} . Since \mathcal{D}_2^{upb} is a jointly convex function of P_k 's (see Appendix VIII-B) we use Lagrange multiplier method and solve the corresponding KKT conditions to find the solution. Also, \mathcal{D}_2^{upb} is a decreasing function of P_k 's and P_{tot} (see Appendix VIII-B). Therefore, solving (SP3) for P_k 's we find:

$$P_k = \left[\frac{L_k}{\gamma_k} \ln\left(\frac{\gamma_k \tau_k^2}{\mu^*} \right) \right]^+, \forall k, \text{ where } \sum_{k=1}^K P_k = P_{tot}, \quad (27)$$

$$\ln \mu^* = \left(\sum_{k \notin \mathcal{J}} \frac{L_k}{\gamma_k} \right)^{-1} [-P_{tot} + \sum_{k \notin \mathcal{J}} \frac{L_k}{\gamma_k} \ln(\gamma_k \tau_k^2)]. \quad (28)$$

Set $\mathcal{J} = \{k : P_k = 0, k = 0, \dots, K\}$ in (28) is the set of inactive sensors: sensors whose $L_k = 0$ or $\gamma_k \tau_k^2 < \mu^*$. It is noteworthy to mention that for asymptotic regime of large P_{tot} , we have the same power allocation policy as in (22).

• **Solving (SP4):** We apply the modified ellipsoid method we used for (SP2), to solve (SP4). The feasible set \mathcal{F} and the update steps are similar, with a difference: the gradient of the objective function $\nabla_{oc}^{(i)}$ changes and instead of $\frac{\partial \mathcal{D}_a}{\partial L_k}, \frac{\partial \mathcal{D}_b}{\partial L_k}$

needs to be derived. However, $\frac{\partial \mathcal{D}_b}{\partial L_k} = \frac{\partial \mathcal{D}_1^{upb}}{\partial L_k} + \frac{\partial \mathcal{D}_2^{upb}}{\partial L_k}$, where:

$$\frac{\partial \mathcal{D}_1^{upb}}{\partial L_k} = \frac{-(\text{tr}(\mathbf{C}_{x\theta}^T \mathbf{C}_{x\theta}))^2 \text{tr}(\mathbf{C}_{x\theta}^T \frac{\partial \mathbf{Q}}{\partial L_k} \mathbf{C}_{x\theta})}{(\text{tr}(\mathbf{C}_{x\theta}^T (\mathbf{C}_x + \mathbf{Q}) \mathbf{C}_{x\theta}))^2},$$

$$\frac{\partial \mathcal{D}_2^{upb}}{\partial L_k} = \begin{cases} \tilde{\lambda} \frac{\partial u_k}{\partial L_k}, & \text{if } k \notin \mathcal{A}, \\ \tilde{\lambda} \left[\frac{\partial u_k}{\partial L_k} - \frac{2 \frac{\partial \sigma_{\epsilon_k}^2}{\partial L_k} \sum_{j=1}^K u_j}{\lambda_{\min}(\mathbf{C}_x) + \sigma_{\epsilon_k}^2} \right], & \text{if } k \in \mathcal{A}, \end{cases}$$

in which set $\mathcal{A} = \{k : k = \underset{i}{\text{argmin}}(\sigma_{\epsilon_i}^2)\}$, $\tilde{\lambda}$ is defined in (15) and

$\frac{\partial \mathbf{Q}}{\partial L_k}, \frac{\partial u_k}{\partial L_k}$ are given in Section IV-A. Having the solutions for (SP3) and (SP4), we can address the problem in (16), when \mathcal{D}_0 is replaced with \mathcal{D}_b , utilizing an iterative algorithm similar to “*a*-coupled” algorithm outlined in Section IV-A, which we call “*b*-coupled” algorithm, and a discretizing approach similar to Section IV-B. Different from “*a*-coupled” algorithm, “*b*-coupled” algorithm does not require matrix inversion, although implementing the modified ellipsoid method still requires a K -dimensional search.

V. “DECOUPLED” SCHEME FOR RESOURCE ALLOCATION

In Section IV we proposed two iterative coupled schemes, which minimize \mathcal{D}_a and \mathcal{D}_b . In both schemes we resorted to the iterative modified ellipsoid method to find L_k 's, since finding a closed-form solution for L_k 's remained elusive. We recall the discussion at the beginning of Section III, which indicates \mathcal{D}_1 (and its bound \mathcal{D}_1^{upb}) represent the MSE due to observation noises and quantization errors, whereas \mathcal{D}_2 (and its bounds $\mathcal{D}_2^{upb}, \mathcal{D}_2^{ubp}$) are the MSE due to communication channel errors. Leveraging on this decoupling of the contributions of observation noises and quantization errors from those of communication channel errors, we propose “decoupled” scheme to minimize these decoupled contributions separately, and to find the optimization parameters $\{L_k, P_k\}_{k=1}^K$ in closed-form expressions, eliminating the computational burden of the modified ellipsoid method for conducting K -dimensional search and finding L^c vector. Similar to Section IV we start with “decoupled” scheme to solve the relaxed problem, via allowing L_k 's to be positive numbers.

A. Decoupled Scheme for Minimizing \mathcal{D}_a

The essence of “decoupled” scheme is to solve the following two sub-problems in a sequential order:

$$\text{(SP5)} \quad \underset{L_k, \forall k}{\text{minimize}} \mathcal{D}_1^{upb}(\{L_k\}_{k=1}^K) \quad (29)$$

$$\text{s.t.} \quad \sum_{k=1}^K L_k \leq B_{tot}, \quad L_k \in \mathbb{R}_+, \quad \forall k,$$

$$\text{(SP6)} \quad \text{given } \{L_k\}_{k=1}^K, \quad \underset{P_k, \forall k}{\text{minimize}} \mathcal{D}_2^{upb}(\{P_k\}_{k=1}^K) \quad (30)$$

$$\text{s.t.} \quad \sum_{k=1}^K P_k \leq P_{tot}, \quad P_k \in \mathbb{R}_+, \quad \forall k.$$

Different from Section IV there is no iteration between (SP5) and (SP6). After solving (SP5) and (SP6), we take a similar approach to Section IV-B, to migrate from continuous to integer solutions for L_k 's.

• **Solving (SP5):** Considering (13), we realize that minimizing \mathcal{D}_1^{upb} is equivalent to minimizing $\text{tr}(\mathbf{C}_{x\theta}^T \mathbf{Q} \mathbf{C}_{x\theta}) = \sum_{k=1}^K \delta_k \sigma_{\epsilon_k}^2$, where δ_k is the squared Euclidean norm of the k -th row of $\mathbf{C}_{x\theta}$. Since $\sum_{k=1}^K \delta_k \sigma_{\epsilon_k}^2$ is a jointly convex function of L_k 's (See Appendix VIII-C) we use Lagrange multiplier method and solve the corresponding KKT conditions to find the solution. Also, $\sum_{k=1}^K \delta_k \sigma_{\epsilon_k}^2$ is a decreasing function of L_k 's and B_{tot} (See Appendix VIII-C). Therefore, solving (SP5) in (29) for L_k 's and using the approximation $2^{L_k} - 1 \approx 2^{L_k}$ we reach:

$$L_k = [\log_2(\sqrt{\frac{\tau_k^2 \delta_k 2 \ln 2}{3\nu^*}})]^+, \quad \forall k \quad \text{where} \quad \sum_{k=1}^K L_k = B_{tot}, \quad (31)$$

$$\nu^* = \frac{2 \ln 2}{3} [4^{-B_{tot}} \prod_{k=1}^K \delta_k \tau_k^2]^{\frac{1}{K}}. \quad (32)$$

Substituting (32) into (31) one can verify:

$$L_k = \left[\frac{B_{tot}}{K} + \log_2 \left(\sqrt{\frac{\delta_k \tau_k^2}{(\prod_{i=1}^K \delta_i \tau_i^2)^{\frac{1}{K}}}} \right) \right]^+, \quad \forall k. \quad (33)$$

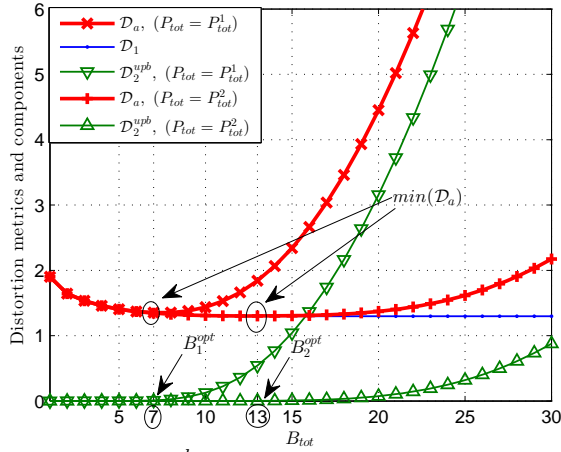
Examining (33), we note that the first term inside the bracket is common among all sensors, whereas the second term differs among sensors and depends on δ_k, τ_k . For $\tau_k = \tau, \forall k$, sensor k with a larger δ_k (i.e., better observation quality) is allocated a larger L_k . Note that, since \mathcal{D}_1^{upb} does not capture communication channel errors, L_k in (33) is independent of sensor communication channel quality. This is different from solution of (SP2) in (18), where L_k 's depend on both sensor observation and communication channel qualities.

• **Solving (SP6):** Similar to (SP1) in (17), the objective function in (30) is a jointly convex function of P_k 's and also decreases as P_k 's and P_{tot} increase (See appendix VIII-B). Indeed, solving (SP6) yields the exact solution as that of (SP1), provided in (20) and (21).

• **Remark 6:** We minimize \mathcal{D}_1^{upb} in (SP5) instead of \mathcal{D}_1 , since it yields a closed form solution for L_k 's given in (33). In Section V-B we discuss minimizing $\mathcal{D}_a = \mathcal{D}_1 + \mathcal{D}_2^{upb}$, when we substitute (33) into \mathcal{D}_1 and (20), (21), (33) into \mathcal{D}_2^{upb} .

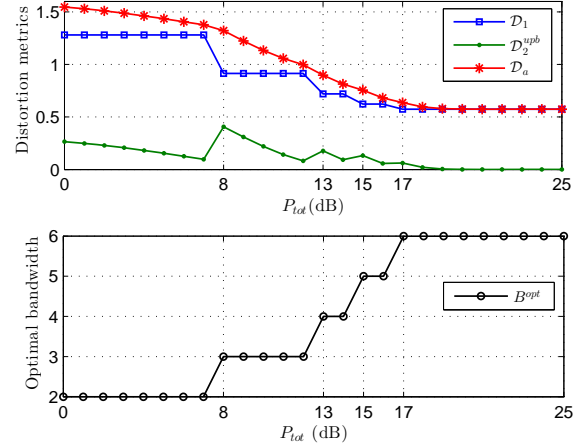
B. Does Depleting B_{tot} always reduce \mathcal{D}_a ?

To answer this question, we consider the solution in (33) for asymptotic regime of large B_{tot} . As $B_{tot} \rightarrow \infty$, we find $L_k \rightarrow \frac{B_{tot}}{K}, \forall k$, i.e., we should equally distribute B_{tot} among sensors. In situations where B_{tot} is large and communication channel quality of sensor k is poor (i.e., small γ_k due to small channel gain $|h_k|$ or small P_k due to low P_{tot}), the solution in (33) can lead to a large value for \mathcal{D}_a , since sending a large number of bits L_k over poor quality channels increases communication channel errors and thus \mathcal{D}_2^{upb} . This observation suggests that perhaps, we should first find B^{opt} (for $B^{opt} < B_{tot}$), where B^{opt} depends on channel gains and P_{tot} , and then distribute B^{opt} among sensors, to control the growth of \mathcal{D}_2^{upb} in \mathcal{D}_a . In fact, when we substitute (33) into \mathcal{D}_1 and (20), (21), (33) into \mathcal{D}_2^{upb} , we find \mathcal{D}_1 is a decreasing function of B_{tot} , whereas \mathcal{D}_2^{upb} is an increasing function of B_{tot} . As $B_{tot} \rightarrow 0$, \mathcal{D}_1 approaches its maximum value $\text{tr}(\mathbf{C}_\theta)$, i.e., trace of covariance of unknowns, whereas \mathcal{D}_2^{upb} goes to


 Fig. 3: $\mathcal{D}_1, \mathcal{D}_2^{upb}, \mathcal{D}_a$ versus B_{tot} (measured in bits)

zero. On the other hand, as $B_{tot} \rightarrow \infty$, \mathcal{D}_1 approaches its minimum value $d_0 = \text{tr}(\mathcal{C}_\theta) - \text{tr}(\mathcal{C}_{x\theta}^T \mathcal{C}_x^{-1} \mathcal{C}_{x\theta})$, i.e., clairvoyant centralized estimation where unquantized sensor observations are available at the FC, whereas \mathcal{D}_2^{upb} grows unboundedly (See Appendix VIII-D). This tradeoff suggests that there should be a value B^{opt} that minimizes \mathcal{D}_a . Fig. 3 illustrates $\mathcal{D}_1, \mathcal{D}_2^{upb}, \mathcal{D}_a$ versus B_{tot} for two values P_{tot}^1, P_{tot}^2 , where $P_{tot}^2 \geq P_{tot}^1$. Fig. 3 shows that $B_2^{opt} \geq B_1^{opt}$. This observation can be explained as the following. Note that \mathcal{D}_1 is independent of P_{tot} , whereas \mathcal{D}_2^{upb} decreases as P_{tot} increases (Appendix VIII-B shows $\frac{\partial \mathcal{D}_2^{upb}}{\partial P_k} \leq 0 \forall k$, and thus $\frac{\partial \mathcal{D}_2^{upb}}{\partial P_{tot}} \leq 0$). Hence, as P_{tot} increases we can transmit a larger number of bits, i.e., larger B^{opt} , without incurring an increase in communication channel errors.

Motivated by these, we propose “ a -decoupled” algorithm. This algorithm starts with initiating $B^{opt} = 1$ and increasing the value of B^{opt} by one bit at each iteration, where the maximum number of iterations is B_{tot} . At iteration i , we find $L_k^{(i)}$ ’s using (33) and $P_k^{(i)}$ ’s using (20),(21), substitute these $L_k^{(i)}, P_k^{(i)}$ ’s into \mathcal{D}_a , and check if the decrease in \mathcal{D}_a in two consecutive iterations is less than zero, i.e., $\mathcal{D}_a(\{L_k^{(i)}, P_k^{(i)}\}_{k=1}^K) - \mathcal{D}_a(\{L_k^{(i-1)}, P_k^{(i-1)}\}_{k=1}^K) < 0$. If this inequality holds for $i < B_{tot}$, we let $B^{opt} = i$ and find the solution for L_k ’s using (33) and P_k ’s using (20), (21), when B_{tot} is substituted with B^{opt} . Otherwise, we let $B^{opt} = B_{tot}$ and find the solution for L_k ’s using (33) and P_k ’s using (20), (21). At the end, we take the approach in Section IV-B to migrate from continuous to integer solutions for rates and find the corresponding powers. Fig. 4 illustrates the behavior of “ a -decoupled” algorithm and in particular, how $B^{opt}, \mathcal{D}_1, \mathcal{D}_2^{upb}, \mathcal{D}_a$ vary as P_{tot} increases. Note that as P_{tot} increases B^{opt} remains constant for certain (long) intervals and increases for some other (short) intervals of P_{tot} values. The behavior of B^{opt} versus P_{tot} dictates the behavior of $\mathcal{D}_1, \mathcal{D}_2^{upb}, \mathcal{D}_a$ as well. For the P_{tot} intervals where B^{opt} is fixed, \mathcal{D}_1 is fixed as well, since it is independent of P_{tot} , whereas \mathcal{D}_2^{upb} and thus \mathcal{D}_a decrease as P_{tot} increases. For the P_{tot} intervals where B^{opt} increases, \mathcal{D}_1 decreases and \mathcal{D}_2^{upb} increases (Appendix VIII-D shows $\frac{\partial \mathcal{D}_1}{\partial B_{tot}} \leq 0$ and $\frac{\partial \mathcal{D}_2^{upb}}{\partial B_{tot}} \geq 0$). Overall, as P_{tot} increases \mathcal{D}_a decreases, since the decrease in \mathcal{D}_1 , when B^{opt} increases, dominates the increase in \mathcal{D}_2^{upb} .


 Fig. 4: behavior of “ a -decoupled” algorithm

Regarding the modified “ a -decoupled” algorithm a remark follows.

• **Remark 7:** The modified “ a -decoupled” algorithm requires only one dimensional search to find B^{opt} and thus L_k ’s (33), as opposed to K -dimensional search required by the modified ellipsoid method in “ a -coupled” algorithm. Also, finding B^{opt} at most needs B_{tot} number of iterations and no switching between solving (SP5) and (SP6) is needed.

C. Decoupled Scheme for Minimizing \mathcal{D}_b

Note that “ a -decoupled” algorithm still requires inversion of matrix $\mathcal{C}_x + \mathbf{Q}$ to calculate α_k and find P_k using (20), (21). To eliminate this matrix inversion, we propose to minimize \mathcal{D}_2^{uupb} instead of \mathcal{D}_2^{upb} . Since \mathcal{D}_2^{uupb} is a jointly convex function of P_k ’s (see Appendix VIII-B), substituting L_k ’s of (33) into \mathcal{D}_2^{uupb} and minimizing it with respect to P_k ’s, we reach the solution provided in (27), (28). Let “ b -decoupled” algorithm be the one that minimizes \mathcal{D}_1^{uupb} and \mathcal{D}_2^{uupb} separately in \mathcal{D}_b . This algorithm is very similar to “ a -decoupled” algorithm described in Section V-B, with the difference that when finding B^{opt} , at iteration i we find $L_k^{(i)}$ ’s using (33) and $P_k^{(i)}$ ’s using (27), (28), substitute these $L_k^{(i)}, P_k^{(i)}$ ’s into \mathcal{D}_b , and check if the decrease in \mathcal{D}_b in two consecutive iterations is less than zero. After finding B^{opt} we find the solution for L_k ’s using (33) and P_k ’s using (27), (28). The behavior of “ b -decoupled” algorithm and in particular, how $B^{opt}, \mathcal{D}_1^{uupb}, \mathcal{D}_2^{uupb}, \mathcal{D}_b$ vary as P_{tot} increases, is similar to “ a -decoupled” algorithm depicted in Fig. 4 and is omitted due to lack of space.

VI. NUMERICAL AND SIMULATION RESULTS

In this section through simulations we corroborate our analytical results. Without loss of generality and for the sake of illustration we set $K = 3$, $\mathcal{C}_\theta = [1 (\sqrt{2}/2); (\sqrt{2}/2) 2]$, $\mathbf{a}_1 = [1 \ 1]^T$, $\mathbf{a}_2 = [0.6 \ 0.6]^T$, $\mathbf{a}_3 = [0.4 \ 0.4]^T$, $\sigma_{n_k}^2 = 1$, $\sigma_{w_k}^2 = 1$, $h_k = 1$, for all algorithms. “CS” and “DS” in the legends of the figures indicate the continuous solutions and discrete solutions of the algorithms, respectively.

Figs. 5 and 6 illustrate $\{10 \log_{10}(P_k)\}_{k=1}^3$ and $\{L_k\}_{k=1}^K$ vs. P_{tot} , respectively, for “ a -coupled” algorithm and $B_{tot} = 30, 3$ bits. Figs.5.a and 6.a for $B_{tot} = 30$ bits (abundant bandwidth) show that as P_{tot} increases, both power and rate allocation approaches uniform allocation. This is in agreement with (22).

When P_{tot} is small, only sensor 1 is active. As P_{tot} increases sensors 2 and 3 become active in sequential order. Figs. 5.b and 6.b for $B_{tot} = 3$ bits (scarce bandwidth) show that only sensor 1 is active and $P_1 = P_{tot}$. Overall, these observations imply that power and rate allocation depends on both P_{tot} and B_{tot} , e.g., when we have plentiful P_{tot} and scarce B_{tot} only the sensor with the largest observation gain is active. Also, uniform power and rate allocation is near optimal when we have ample P_{tot} and B_{tot} .

Figs. 7 and 8 depict $\{10 \log_{10}(P_k)\}_{k=1}^3$ and $\{L_k\}_{k=1}^K$ vs. P_{tot} , respectively, for “ a -decoupled” algorithm and $B_{tot} = 30, 3$ bits. Similar to “ a -coupled” algorithm, we observe that when both P_{tot} and B_{tot} are abundant, uniform power and rate allocation is near optimal. This is in agreement with (22), (33). On the other hand, when B_{tot} is scarce, power and rate allocation is way different from being uniform. In fact, when P_{tot} is ample, (22) indicates that P_k is proportional to L_k . Also, when B_{tot} is scarce, (33) states that L_k 's and consequently P_k 's are not uniformly distributed. These indicate that power and rate allocation is affected by sensors' observation qualities and channel gains, as well as both P_{tot} and B_{tot} . There are two slight differences between “ a -coupled” and “ a -decoupled” algorithms: (i) for $B_{tot} = 30$ bits (ample bandwidth) sensors 2 and 3 become active at smaller P_{tot} values in “ a -decoupled” algorithm, (ii) for $B_{tot} = 3$ bits (scarce bandwidth), “ a -decoupled” algorithm ultimately activates all sensors at P_{tot} increases, while “ a -coupled” algorithm only activates sensor 1. Note that for scarce bandwidth, even when P_{tot} is very large, power and rate allocation in “ a -decoupled” algorithm is non-uniform.

Figs. 9 and 10 depict $\{10 \log_{10}(P_k)\}_{k=1}^3$ and $\{L_k\}_{k=1}^K$ vs. B_{tot} , respectively, for “ a -coupled” algorithm and $P_{tot} = 16, 30$ dB. The observations in these figures are in full agreement with the former ones. In particular, for $P_{tot} = 30$ dB (large power), when B_{tot} is small, only sensor 1 is active. As B_{tot} increases, sensors 2 and 3 become active too, in a way that power and rate allocation approaches to uniform for large B_{tot} . On the other hand, for $P_{tot} = 16$ dB only sensor 1 is active and $P_1 = P_{tot}$.

Figs. 11 and 12 illustrate $\{10 \log_{10}(P_k)\}_{k=1}^3$ and $\{L_k\}_{k=1}^K$ vs. B_{tot} , respectively, for “ a -decoupled” algorithm and $P_{tot} = 16, 30$ dB. While the behaviors of “ a -coupled” and “ a -decoupled” have similarities, they have differences as the following: (i) for $P_{tot} = 30$ dB sensors 2 and 3 become active at smaller B_{tot} value in “ a -decoupled” algorithm, (ii) for $P_{tot} = 16$ dB, “ a -decoupled” algorithm ultimately activates all sensors as B_{tot} increases, while “ a -coupled” algorithm only activates sensor 1. Note for $P_{tot} = 16$ dB, even when B_{tot} is very large, power and rate allocation in “ a -decoupled” algorithm is non-uniform. this is because $B^{opt} < B_{tot}$ in this case and according to (33), (20), (21) power and rate allocation would be non-uniform.

In Fig. 13 we plot \mathcal{D}_a when implementing “ a -coupled” and “ a -decoupled” and \mathcal{D}_b when implementing “ b -coupled” and “ b -decoupled” algorithms, vs. P_{tot} , for $B_{tot} = 30, 3$ bits. We observe that “ a -coupled” and “ b -decoupled” algorithms perform the best and the worst, respectively. Also, All the algorithms outperform uniform resource allocation (except for

“ b -decoupled” algorithm when $B_{tot} = 3$ bits and $13 < P_{tot} < 18$ dB). For small P_{tot} , the performance of each algorithm does not change as we decrease $B_{tot} = 30$ bits to $B_{tot} = 3$ bits.

This observation can be explained as the following. For small P_{tot} , the communication channels cannot support reliable transmission of large number of bits. Hence, the algorithms allocate few bits to sensors and increasing B_{tot} does not improve the performance. Another observation is that for $B_{tot} = 30$ bits (plentiful bandwidth) and large P_{tot} , performance of all algorithms reaches the clairvoyant benchmark d_0 , whereas for $B_{tot} = 3$ bits (scarce bandwidth) and large P_{tot} there is a persistent gap with d_0 for each algorithm, due to quantization errors, and “ a -coupled” and “ b -decoupled” algorithms perform the best and the worst, respectively.

Fig. 14 depicts the Mont Carlo simulated MSE when “ a -coupled”, “ b -coupled”, “ a -decoupled” and “ b -decoupled” algorithms are implemented for power and rate allocation vs. P_{tot} for $B_{tot} = 30, 3$ bits. Similar observations to those of Fig. 13 are made, with a few differences: (i) “ b -coupled” outperforms “ a -decoupled” algorithm in very low P_{tot} , (ii) the simulated MSE obtained by “ b -coupled”, “ a -decoupled”, and “ b -decoupled” algorithms approaches the same value for $B_{tot} = 3$ bits and large P_{tot} . The reason perhaps is that the discretized quantization rates are the same for these algorithms and according to (22) for large P_{tot} , P_k 's of these algorithms become identical.

To better see the behavior of the upper bounds with respect to the simulated MSE, Figs. 15 and 16 plot the simulated MSE and upper bounds vs. P_{tot} , for all the proposed algorithms (note that Figs. 15 and 16 have the same curves as Figs. 13 and 14). We observe that when P_{tot} and B_{tot} are not too low, the upper bounds are good approximations of the simulated MSE.

Fig. 17 depicts \mathcal{D}_a when implementing “ a -coupled” and “ a -decoupled” and \mathcal{D}_b when implementing “ b -coupled” and “ b -decoupled” algorithms, vs. B_{tot} , for $P_{tot} = 30, 16$ dB.

Fig. 18 depicts the simulated MSE when “ a -coupled”, “ b -coupled”, “ a -decoupled” and “ b -decoupled” algorithms are implemented for power and rate allocation vs. B_{tot} for $P_{tot} = 30, 16$ dB. We make similar observations and conclusions to those we made for Fig. 14. For $P_{tot} = 30$ dB and large B_{tot} , performance of all algorithms reaches the clairvoyant benchmark d_0 . On the other hand, for $P_{tot} = 16$ dB and large B_{tot} , there is a persistent gap with d_0 for each algorithm, due to communication channel errors. When comparing Figs. 17 and 18, we note that the behavior of the bounds \mathcal{D}_a and \mathcal{D}_b vs. B_{tot} is very similar to that of the simulated MSE.

VII. CONCLUSIONS

We considered distributed estimation of a Gaussian vector with a known covariance matrix and linear observation model, where the FC is tasked with reconstruction of the unknowns, using a linear estimator. Sensors employ uniform multi-bit quantizers and BPSK modulation, and communicate with the FC over power- and bandwidth-constrained channels. We derived two closed-form upper bounds on the MSE, in terms of the optimization parameters (i.e., transmit power and quantization rate per sensor). Each bound consists of two

terms, where the first term is the MSE due to observation noises and quantization errors, and the second term is the MSE due to communication channel errors. We proposed ‘‘coupled’’ and ‘‘decoupled’’ resource allocation schemes that minimize these bounds. The ‘‘coupled’’ schemes utilize the iterative modified ellipsoid method to conduct K -dimensional search and find the quantization rate vector, whereas the ‘‘decoupled’’ ones rely on one-dimensional search to find the quantization rates. Our simulations show that when P_{tot} and B_{tot} are not too scarce, the bounds are good approximations of the actual MSE. Through simulations, we verified the effectiveness of the proposed schemes and confirmed that their performance approaches the clairvoyant centralized estimation for large P_{tot} and B_{tot} ($P_{tot} \approx 25$ dB, $B_{tot} \approx 30$ bits). Our results indicate that resource allocation is affected by sensors’ observation qualities, channel gains, as well as P_{tot} and B_{tot} , e.g., two WSNs with identical conditions and P_{tot} (B_{tot}) and different B_{tot} (P_{tot}) require two different power (rate) allocation. Also, more number of bits and transmit power are allotted to sensors with better observation qualities.

VIII. APPENDIX

A. Finding Upper Bound on $\mathbb{E}\{(\hat{m}_k - m_k)^2\}$

Suppose the bit sequence representations of m_k and \hat{m}_k are, respectively, $(b_{k,1}, \dots, b_{k,L_k})$ and $(\hat{b}_{k,1}, \dots, \hat{b}_{k,L_k})$, i.e., $m_k = \Delta_k(0.5 - 2^{L_k-1} + \sum_{j=1}^{L_k} b_{k,j} 2^{L_k-j})$ and $\hat{m}_k = \Delta_k(0.5 - 2^{L_k-1} + \sum_{j=1}^{L_k} \hat{b}_{k,j} 2^{L_k-j})$. Therefore:

$$\begin{aligned} \mathbb{E}\{(\hat{m}_k - m_k)^2\} &= \Delta_k^2 \mathbb{E}\left\{\left(\sum_{j=1}^{L_k} 2^{L_k-j} (b_{k,j} - \hat{b}_{k,j})\right)^2\right\} \\ &\stackrel{(a)}{\leq} \Delta_k^2 L_k (4^{L_k}) \sum_{j=1}^{L_k} 4^{-j} \underbrace{\mathbb{E}\{(b_{k,j} - \hat{b}_{k,j})^2\}}_{=p_e} \\ &\stackrel{(b)}{=} p_e \Delta_k^2 L_k (4^{L_k}) \frac{1 - (1/4)^{L_k}}{3} \\ &\stackrel{(c)}{<} \frac{4p_e L_k \tau_k^2}{3} \stackrel{(d)}{\leq} \exp\left(-\frac{\gamma_k P_k}{L_k}\right) \frac{4L_k \tau_k^2}{3} \end{aligned}$$

where (a) comes from Cauchy’s inequality $(\sum_j \alpha_j \beta_j)^2 \leq (\sum_j \alpha_j^2)(\sum_j \beta_j^2)$ for arbitrary α_j, β_j ’s, and the fact that $(b_{k,j} - \hat{b}_{k,j})^2$ is a Bernoulli random variable with success probability p_e , (b) is due to sum of a geometric series, (c) is found using the definition of Δ_k and $1 - (1/4)^{L_k} < 1$, and (d) is obtained since $p_e = \mathcal{Q}(\sqrt{\frac{2\gamma_k P_k}{L_k}})$ and $\mathcal{Q}(x) \leq \exp(-\frac{x^2}{2})$.

B. Properties of \mathcal{D}_2^{upb} and \mathcal{D}_2^{uupb}

One can verify the following:

$$\begin{aligned} \frac{\partial \mathcal{D}_2^{upb}}{\partial P_k} &= -\alpha_k \gamma_k \exp\left(-\frac{\gamma_k P_k}{L_k}\right) \leq 0, \quad \forall k \\ \frac{\partial^2 \mathcal{D}_2^{upb}}{\partial P_k \partial P_l} &= \begin{cases} 0, & \text{if } k \neq l \\ \frac{\alpha_k \gamma_k^2}{L_k} \exp\left(-\frac{\gamma_k P_k}{L_k}\right) \geq 0, & \text{if } k = l \end{cases} \end{aligned}$$

These imply that \mathcal{D}_2^{upb} is a decreasing function of P_k ’s and also a jointly convex function of P_k ’s. Similarly:

$$\begin{aligned} \frac{\partial \mathcal{D}_2^{uupb}}{\partial P_k} &= \tilde{\lambda} \left[\frac{\partial \mathcal{M}'}{\partial P_k} \right]_{k,k} = -\tilde{\lambda} \left(\frac{4\tau_k^2 \gamma_k}{3} \right) \exp\left(-\frac{\gamma_k P_k}{L_k}\right) \leq 0, \quad \forall k \\ \frac{\partial^2 \mathcal{D}_2^{uupb}}{\partial P_k \partial P_l} &= \begin{cases} 0, & \text{if } k \neq l \\ \tilde{\lambda} \left(\frac{4\tau_k^2 \gamma_k^2}{3L_k} \right) \exp\left(-\frac{\gamma_k P_k}{L_k}\right) \geq 0, & \text{if } k = l \end{cases} \end{aligned}$$

These imply that \mathcal{D}_2^{uupb} is a decreasing function of P_k ’s and also a jointly convex function of P_k ’s.

C. Properties of $\sum_{k=1}^K \delta_k \sigma_{\epsilon_k}^2$

One can verify the following:

$$\begin{aligned} \frac{\partial (\sum_{k=1}^K \delta_k \sigma_{\epsilon_k}^2)}{\partial L_k} &= -\frac{2 \ln 2 \delta_k \tau_k^2 2^{L_k}}{3(2^{L_k} - 1)^3} \leq 0, \quad \forall k \\ \frac{\partial^2 (\sum_{k=1}^K \delta_k \sigma_{\epsilon_k}^2)}{\partial L_k \partial L_l} &= \begin{cases} 0, & \text{if } k \neq l \\ \frac{(\ln 2)^2 \delta_k \tau_k^2 2^{L_k+1} (1+2^{L_k+1})}{3(2^{L_k} - 1)^4} \geq 0, & \text{if } k = l \end{cases} \end{aligned}$$

These imply that $\sum_{k=1}^K \delta_k \sigma_{\epsilon_k}^2$ is a decreasing function of L_k ’s and also a jointly convex function of L_k ’s.

D. More Properties on \mathcal{D}_1 and \mathcal{D}_2^{upb}

• \mathcal{D}_1 is a decreasing function of B_{tot} : after some mathematical manipulations, one can show

$$\frac{\partial \mathcal{D}_1}{\partial B_{tot}} = \text{tr}(\mathbf{G} \frac{\partial \mathbf{Q}}{\partial B_{tot}} \mathbf{G}^T) = \sum_{k=1}^K \left[\frac{\partial \mathbf{Q}}{\partial B_{tot}} \right]_{k,k} \|\mathbf{g}_k\|^2 \leq 0,$$

where after substituting (33) into \mathbf{Q} we find $[\frac{\partial \mathbf{Q}}{\partial B_{tot}}]_{k,k} = -\frac{2 \ln 2 \tau_k^2 2^{L_k}}{3(2^{L_k} - 1)^3 K} \leq 0$. As $B_{tot} \rightarrow 0$, $[\mathbf{Q}]_{k,k} \rightarrow \infty$, i.e., all eigenvalues of $(\mathcal{C}_x + \mathbf{Q})$ go to infinity. Consequently, due to Weyl’s inequality [24] all eigenvalues of $(\mathcal{C}_x + \mathbf{Q})^{-1}$ go to zero. Since $(\mathcal{C}_x + \mathbf{Q})^{-1}$ is a diagonalizable matrix, this means $(\mathcal{C}_x + \mathbf{Q})^{-1}$ goes to an all-zero matrix and $\mathcal{D}_1 \rightarrow \text{tr}(\mathcal{C}_\theta)$. On the other hand, as $B_{tot} \rightarrow \infty$, $[\mathbf{Q}]_{k,k} \rightarrow 0$ and thus $\mathcal{D}_1 \rightarrow d_0 = \text{tr}(\mathcal{C}_\theta) - \text{tr}(\mathcal{C}_{x\theta}^T \mathcal{C}_x^{-1} \mathcal{C}_{x\theta})$.

• \mathcal{D}_2^{upb} is an increasing function of B_{tot} : after some mathematical manipulations, one can verify

$$\frac{\partial \mathcal{D}_2^{upb}}{\partial B_{tot}} = \text{tr}(\mathbf{G} \frac{\partial \mathcal{M}'}{\partial B_{tot}} \mathbf{G}^T) + \text{tr}(\mathbf{G}(\mathbf{B} + \mathbf{B}^T) \mathbf{G}^T), \quad (34)$$

where $\mathbf{B} = -(\frac{\partial \mathbf{Q}}{\partial B_{tot}})(\mathcal{C}_x + \mathbf{Q})^{-1} \mathcal{M}'$. Substituting (33) into \mathcal{M}' we find $[\frac{\partial \mathcal{M}'}{\partial B_{tot}}]_{k,k} = \frac{\partial u_k}{\partial B_{tot}} = \frac{4\tau_k^2}{3K} \exp\left(-\frac{\gamma_k P_k}{L_k}\right) \left[1 + \frac{\gamma_k P_k}{L_k}\right] \geq 0$. Hence, $\mathbf{G} \frac{\partial \mathcal{M}'}{\partial B_{tot}} \mathbf{G}^T \geq 0$ and the first term in (34) is non-negative. Next we show that the second term in (34) is also non-negative and hence $\frac{\partial \mathcal{D}_2^{upb}}{\partial B_{tot}} \geq 0$. Since $\mathbf{G}^T \mathbf{G}$ and $\mathbf{B} + \mathbf{B}^T$ are symmetric matrices and $\mathbf{G}^T \mathbf{G} \geq 0$, using inequality (2) of [27] we obtain:

$$\text{tr}(\mathbf{G}(\mathbf{B} + \mathbf{B}^T) \mathbf{G}^T) = \text{tr}(\mathbf{G} \mathbf{G}^T (\mathbf{B} + \mathbf{B}^T)) \geq \lambda_{\min}(\mathbf{G} \mathbf{G}^T) \text{tr}(\mathbf{B} + \mathbf{B}^T)$$

where $\lambda_{\min}(\mathbf{G} \mathbf{G}^T) \geq 0$. Furthermore,

$$\begin{aligned} \text{tr}(\mathbf{B} + \mathbf{B}^T) &= 2\text{tr}(\mathbf{B}) = 2\text{tr}(\mathcal{M}'(-\frac{\partial \mathbf{Q}}{\partial B_{tot}})(\mathcal{C}_x + \mathbf{Q})^{-1}) \\ &\stackrel{(e)}{\geq} 2\lambda_{\min}(\mathcal{M}'(-\frac{\partial \mathbf{Q}}{\partial B_{tot}})) \text{tr}((\mathcal{C}_x + \mathbf{Q})^{-1}) \stackrel{(f)}{\geq} 0 \end{aligned}$$

in which (e), (f) above are found since $\mathcal{M}'(-\frac{\partial \mathcal{Q}}{\partial B_{tot}})$ and $(\mathcal{C}_x + \mathcal{Q})^{-1}$ are symmetric and positive definite matrices. As $B_{tot} \rightarrow 0$, $[\mathcal{M}']_{k,k} \rightarrow 0$ and \mathbf{G}, \mathbf{G}^T go to all-zero matrices and therefore $\mathcal{D}_2^{upb} \rightarrow 0$. On the other hand, as $B_{tot} \rightarrow \infty$, $[\mathcal{M}']_{k,k} \rightarrow \infty$ and $\mathbf{G} \rightarrow \mathcal{C}_x^T \theta \mathcal{C}_x^{-1}$ and therefore $\mathcal{D}_2^{upb} \rightarrow \infty$.

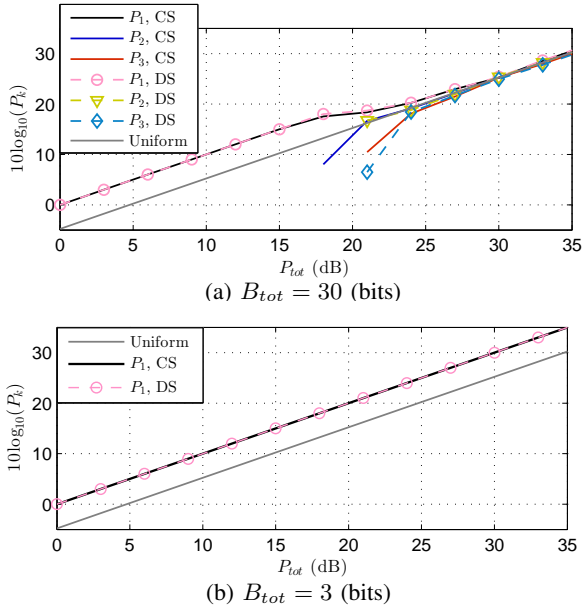


Fig. 5: “a-coupled” algorithm $\{10 \log_{10}(P_k)\}_{k=1}^3$ vs. P_{tot}

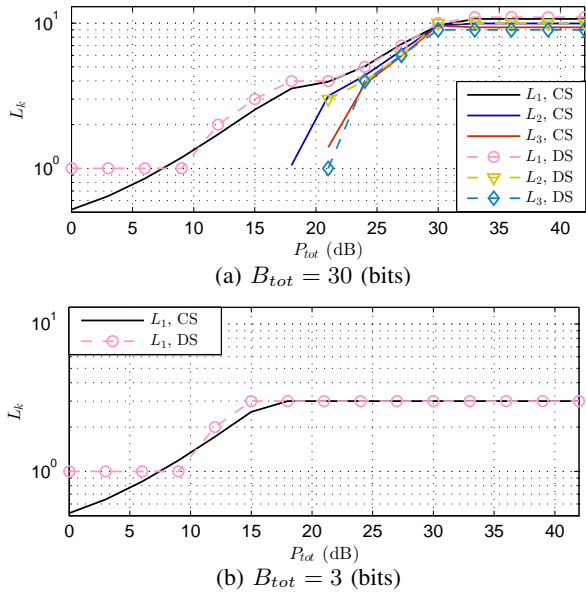


Fig. 6: “a-coupled” algorithm $\{L_k\}_{k=1}^3$ vs. P_{tot}

ACKNOWLEDGMENT

This research is supported by NSF under grants CCF-1336123, CCF-1341966, and CCF-1319770.

REFERENCES

[1] A. Sani and A. Vosoughi, “Resource allocation optimization for distributed vector estimation with digital transmission,” in *Signals, Systems and Computers, 2014 48th Asilomar Conference on*, Nov 2014, pp. 1463–1467.

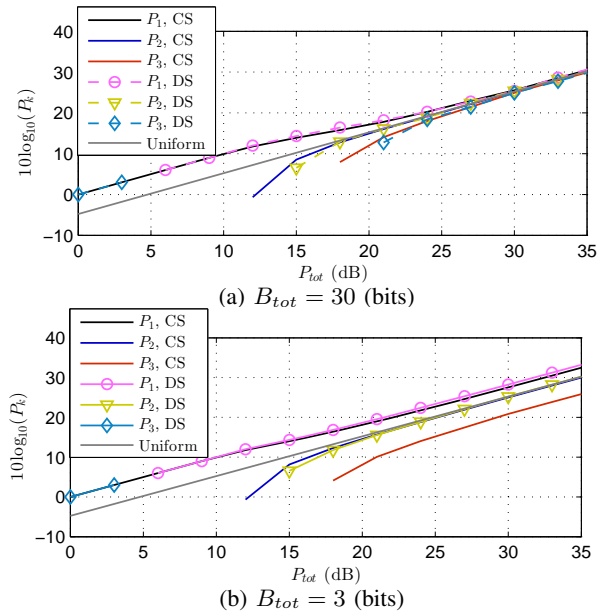


Fig. 7: “a-decoupled” algorithm $\{10 \log_{10}(P_k)\}_{k=1}^3$ vs. P_{tot}

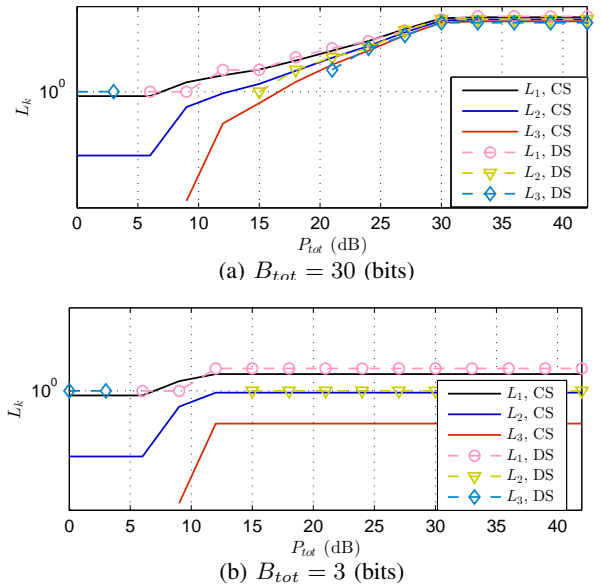


Fig. 8: “a-decoupled” algorithm $\{L_k\}_{k=1}^K$ vs. P_{tot}

[2] —, “Bandwidth and power constrained distributed vector estimation in wireless sensor networks,” in *Military Communications Conference (MILCOM), 2015 IEEE*, Oct 2015, accepted.

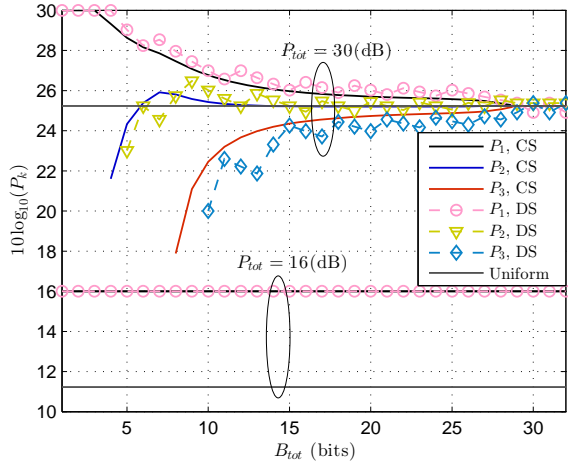
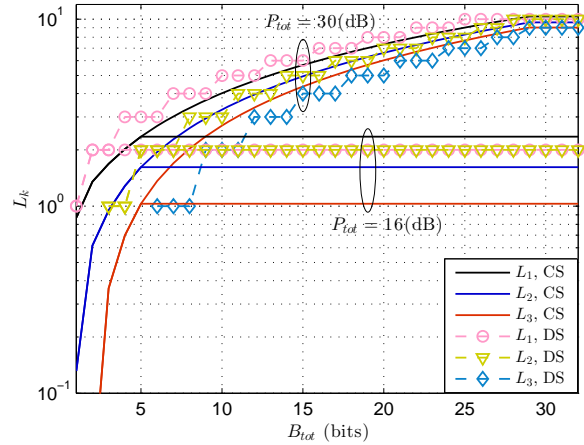
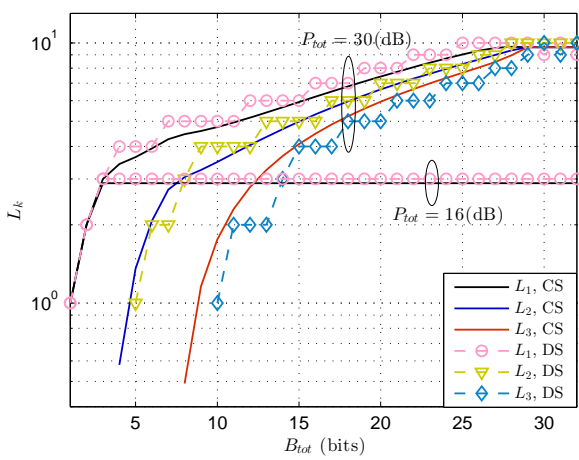
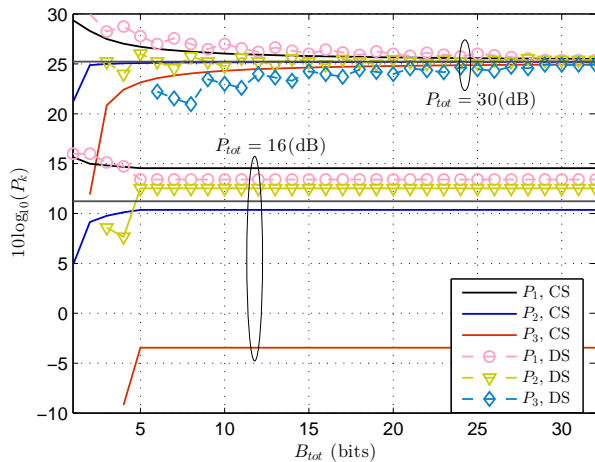
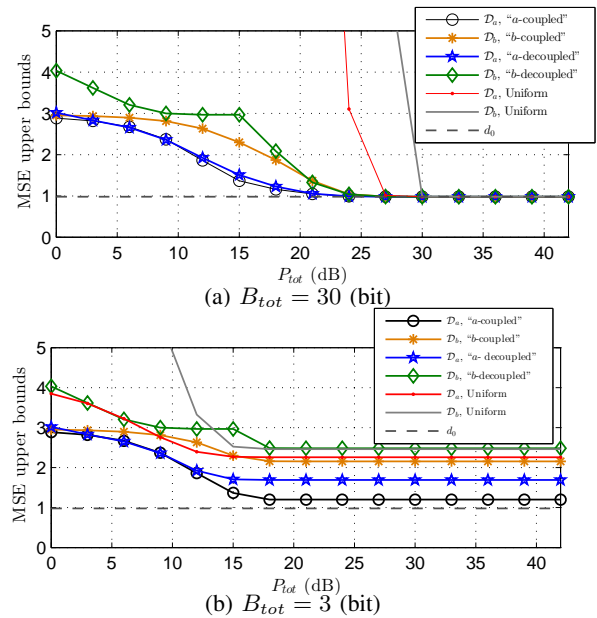
[3] A. Vempaty, H. He, B. Chen, and P. Varshney, “On quantizer design for distributed bayesian estimation in sensor networks,” *Signal Processing, IEEE Transactions on*, vol. 62, no. 20, pp. 5359–5369, Oct 2014.

[4] A. Ribeiro and G. Giannakis, “Bandwidth-constrained distributed estimation for wireless sensor networks-part i: Gaussian case,” *Signal Processing, IEEE Transactions on*, vol. 54, no. 3, pp. 1131–1143, March 2006.

[5] —, “Bandwidth-constrained distributed estimation for wireless sensor networks-part ii: unknown probability density function,” *Signal Processing, IEEE Transactions on*, vol. 54, no. 7, pp. 2784–2796, July 2006.

[6] S. Marano, V. Matta, and P. Willett, “Quantizer precision for distributed estimation in a large sensor network,” *Signal Processing, IEEE Transactions on*, vol. 54, no. 10, pp. 4073–4078, Oct 2006.

[7] J. Li and G. AlRegib, “Rate-constrained distributed estimation in wireless sensor networks,” *Signal Processing, IEEE Transactions on*, vol. 55, no. 5, pp. 1634–1643, May 2007.


 Fig. 9: “a-coupled” algorithm $\{10 \log_{10}(P_k)\}_{k=1}^3$ vs. B_{tot}

 Fig. 12: “a-decoupled” algorithm $\{L_k\}_{k=1}^K$ vs. B_{tot}

 Fig. 10: “a-coupled” algorithm $\{L_k\}_{k=1}^K$ vs. B_{tot}

 Fig. 11: “a-decoupled” algorithm $\{10 \log_{10}(P_k)\}_{k=1}^3$ vs. B_{tot}

 Fig. 13: \mathcal{D}_a and \mathcal{D}_b vs. P_{tot} for all algorithms

March 2014.

- [8] H. Chen and P. Varshney, “Performance limit for distributed estimation systems with identical one-bit quantizers,” *Signal Processing, IEEE Transactions on*, vol. 58, no. 1, pp. 466–471, Jan 2010.
- [9] S. Kar, H. Chen, and P. Varshney, “Optimal identical binary quantizer design for distributed estimation,” *Signal Processing, IEEE Transactions on*, vol. 60, no. 7, pp. 3896–3901, July 2012.
- [10] S. Talarico, N. Schmid, M. Alkhweldi, and M. Valenti, “Distributed estimation of a parametric field: Algorithms and performance analysis,” *Signal Processing, IEEE Transactions on*, vol. 62, no. 5, pp. 1041–1053,

- [11] I. Nevat, G. Peters, and I. Collings, “Random field reconstruction with quantization in wireless sensor networks,” *Signal Processing, IEEE Transactions on*, vol. 61, no. 23, pp. 6020–6033, Dec 2013.
- [12] J.-J. Xiao, S. Cui, Z.-Q. Luo, and A. Goldsmith, “Power scheduling of universal decentralized estimation in sensor networks,” *Signal Processing, IEEE Transactions on*, vol. 54, no. 2, pp. 413–422, Feb 2006.
- [13] J. Li and G. AlRegib, “Distributed estimation in energy-constrained wireless sensor networks,” *Signal Processing, IEEE Transactions on*, vol. 57, no. 10, pp. 3746–3758, Oct 2009.
- [14] X. Luo and G. Giannakis, “Energy-constrained optimal quantization for wireless sensor networks,” *EURASIP J. Adv. Signal Process.*, p. 12, 2008.
- [15] I. Bahceci and A. Khandani, “Linear estimation of correlated data in wireless sensor networks with optimum power allocation and analog modulation,” *Communications, IEEE Transactions on*, vol. 56, no. 7, pp. 1146–1156, July 2008.
- [16] J. Fang and H. Li, “Hyperplane-based vector quantization for distributed estimation in wireless sensor networks,” *Information Theory, IEEE Transactions on*, vol. 55, no. 12, pp. 5682–5699, Dec 2009.
- [17] A. Behbahani, A. Eltawil, and H. Jafarkhani, “Decentralized estimation under correlated noise,” *Signal Processing, IEEE Transactions on*, vol. 62, no. 21, pp. 5603–5614, Nov 2014.
- [18] —, “Linear decentralized estimation of correlated data for power-

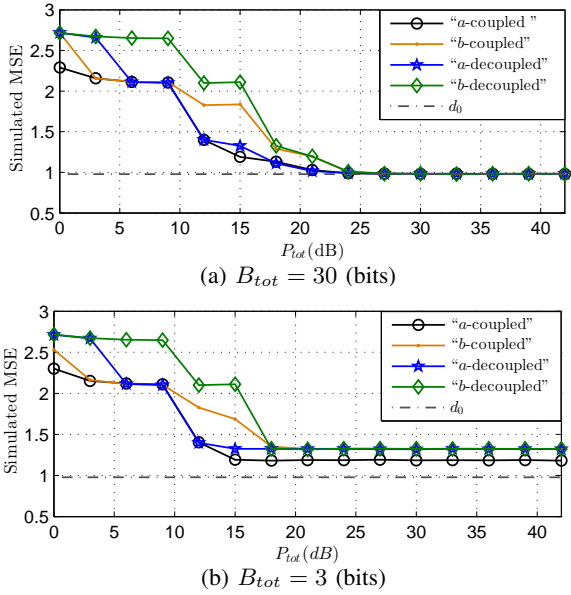


Fig. 14: Simulated MSE vs. P_{tot} for all algorithms

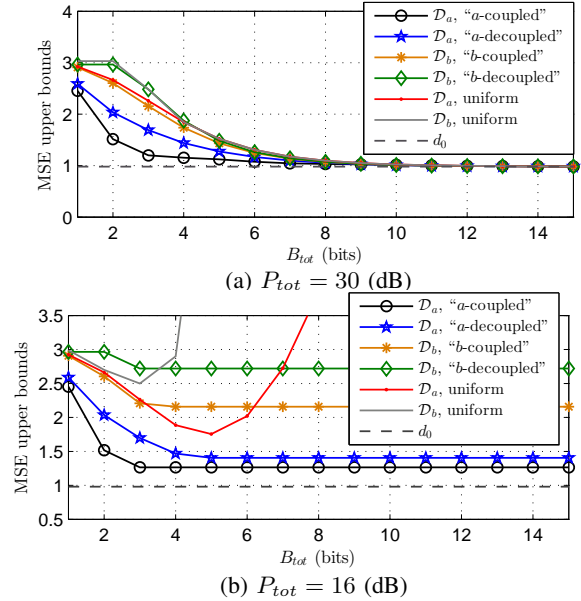


Fig. 17: D_a and D_b vs. B_{tot} for all algorithms

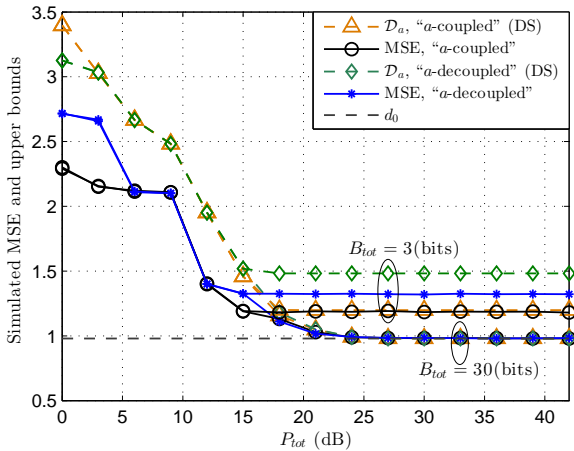


Fig. 15: Simulated MSE and D_a vs. P_{tot} for "a-coupled" and "a-decoupled" algorithms

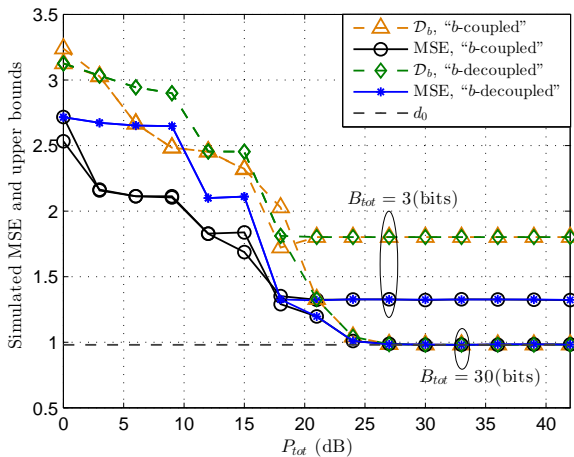


Fig. 16: Simulated MSE and D_b vs. P_{tot} , for "b-coupled" and "b-decoupled" algorithms

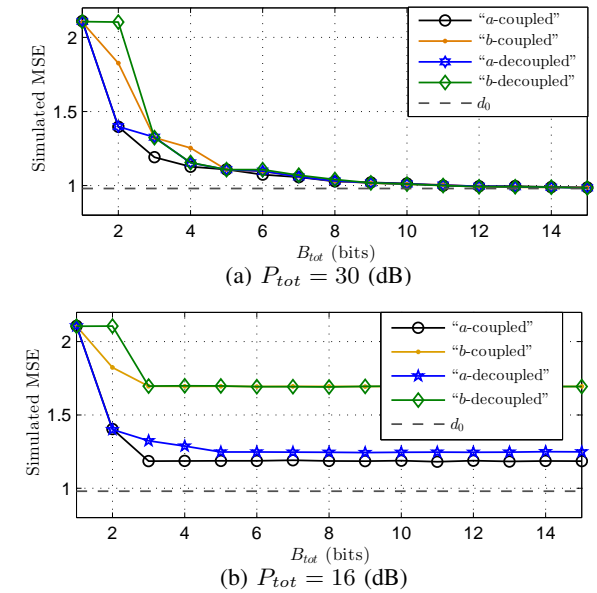


Fig. 18: Simulated MSE vs. B_{tot} for all algorithms

constrained wireless sensor networks," *Signal Processing, IEEE Transactions on*, vol. 60, no. 11, pp. 6003–6016, Nov 2012.

- [19] M. Ahmed, T. Al-Naffouri, M.-S. Alouini, and G. Turkiyyah, "The effect of correlated observations on the performance of distributed estimation," *Signal Processing, IEEE Transactions on*, vol. 61, no. 24, pp. 6264–6275, Dec 2013.
- [20] S. Kay, *Fundamentals of statistical signal processing: estimation theory*. Prentice Hall, Upper Saddle River, NJ, 1993.
- [21] B. Widrow and I. Kollar, *Quantization Noise: Roundoff Error in Digital Computation, Signal Processing, Control and Communications*. Cambridge Univ. Press, 2008.
- [22] A. Vosoughi and A. Scaglione, "Everything you always wanted to know about training: guidelines derived using the affine precoding framework and the crb," *Signal Processing, IEEE Transactions on*, vol. 54, no. 3, pp. 940–954, March 2006.
- [23] F. Zhang and Q. Zhang, "Eigenvalue inequalities for matrix product," *Automatic Control, IEEE Transactions on*, vol. 51, no. 9, pp. 1506–1509, Sept 2006.

- [24] R. Bhatia, *Matrix Analysis, Graduate Texts in Mathematics*. Springer, 1997.
- [25] D. Li and X. Sun, *Nonlinear Integer Programming*. Springer, 2006.
- [26] S. Boyd, "Convex optimization," University Lecture, 2008.
- [27] J. Baksalary and S. Puntanen, "An inequality for the trace of matrix product," *Automatic Control, IEEE Transactions on*, vol. 37, no. 2, pp. 239–240, Feb 1992.